Advances in Colloid and Interface Science 294 (2021) 102455

Contents lists available at ScienceDirect

Advances in Colloid and Interface Science

journal homepage: www.elsevier.com/locate/cis

Historical Perspective

Emulsions in external electric fields

Johan Sjöblom [a], Sameer Mhatre [b,*], Sébastien Simon [a,**], Roar Skartlien [a,c], Geir Sørland [a,d]

[a] Ugelstad Laboratory, Norwegian University of Science and Technology, 7491 Trondheim, Norway
[b] Department of Chemical and Petroleum Engineering, Schulich School of Engineering, University of Calgary, Calgary T2N 1N4, Canada
[c] Institute for Energy Technology (IFE), P.O. Box 40, N-2027 Kjeller, Norway
[d] Anvendt Teknologi AS, Munkvollvegen 56, 7022 Trondheim, Norway

ARTICLE INFO

Keywords:
Electrocoalescence
Crude-oil Emulsions
Phase separation
Demulsification
Dehydration
Chemical demulsifiers
Dissipative particle dynamics (DPD)
Low-field nuclear magnetic resonance (LF-NMR)

ABSTRACT

Water is co-produced with crude oils, generally in the form of water-in-crude oil emulsions. The oil and water phases need to be separated before export. Separation is performed in gravity separators with the addition of chemical demulsifiers and, sometimes, with the application of an electric field by using an electrocoalescer. The present article reviews several aspects of electrocoalescence by considering the effect of the electric field from the molecular to a macroscopic scale: the oil-water interface, single drop effects, two drop interactions, and finally emulsions at laboratory scales. Experimental results together with Dissipative Particle Dynamics (DPD) simulation results are presented.

The review begins with water-oil interface under an electric field and followed by single drop electrohydrodynamics. The electric field is shown to influence the adsorption of crude oil indigenous surface-active components (asphaltenes) due to the electrohydrodynamic (EHD) flows. The interactions between two droplets in the presence of electric field and the factors governing the drop-drop coalescence are discussed in detail.

DPD simulations help to elucidate thin film breakup during (electro)-coalescence of two water droplets, where the oil film has drained out to nanometer thickness. The film is comprised of surfactant and demulsifier molecules, and the simulations capture the pores formation in the film when a DC field is applied. The results demonstrate influence of the molecular structure of the surfactant and demulsifier, and their interactions.

The subsequent section describes experimental techniques to assess the resolution of crude oil emulsions at the laboratory scale. The focus is on low-field Nuclear Magnetic Resonance (LF-NMR) which allows a determination of various emulsion features such as the droplet size distribution (DSD) and the brine profile (variation of the concentration of water with the height of the emulsion sample) and their evolution with time. Application of the technique in emulsion treatment involving chemical demulsifiers and electric field is presented. The review concludes with description of commercial industrial electrocoalecers such as the Vessel Internal Electrostatic Coalescer (VIEC) and the Compact Electrostatic Coalescer (CEC).

1. Introduction

It is well known that water-in-oil emulsions with stabilized water droplets constitute a process problem for crude oil exploration offshore [1,2]. The emulsions need to be resolved in order to separate oil and water and the maximum allowed water content in the export crude oil phase is 0.5 wt%. In crude oil, there are indigenous stabilizers that give natural emulsion stability without addition of chemicals. These components are naphthenic acid [3] and asphaltene fractions, the latter defined by their propensity to precipitate in solutions of higher alkanes, like pentane and heptane [4,5]. Their solubility is very limited and depends on external parameters like temperature, pressure and molecular composition of the hydrocarbon phase [4].

There has been an extreme interest in the structure and chemistry of these hydrophobic but polar components [6], and the background for this is in the vast technological importance and economical impact. Another background is the complex structure of asphaltenes. A definite structure has not been possible to identify despite of intense research

* Corresponding author.
** Corresponding author at: Ugelstad Laboratory, Department of Chemical Engineering, The Norwegian University of Science and Technology (NTNU), N-7491 Trondheim, Norway.
E-mail addresses: sameer.e.mhatre@gmail.com (S. Mhatre), sebastien.simon@chemeng.ntnu.no (S. Simon).

https://doi.org/10.1016/j.cis.2021.102455
Received in revised form 25 May 2021;
Available online 30 May 2021
0001-8686/© 2021 The Author(s). Published by Elsevier B.V. This is an open access article under the CC BY license (http://creativecommons.org/licenses/by/4.0/).

[6–8], and the main challenge lie in the polydispersity and self-association properties [9]. A more practical approach has been to map the asphaltenic properties at oil/water interfaces [10–13] and to characterize the asphaltene fraction according to total functionality with contributions from all individual species. This has been the traditional characterization approach. For electrocoalescence, an understanding of the changes in the properties of an oil-water interface when an electric field is applied is very central for improving the efficiency of this important technology under practical operational conditions.

The water/crude oil interface is highly complex due to the polar molecules in oil which have an affinity for the interface. The most natural approach to understand the chemistry of the components would be to isolate them in the bulk according to some chromatographic methods or directly characterizing them by powerful mass spectrometry techniques such as the Fourier transform ion cyclotron resonance mass spectrometry, FT- ICR MS. The latter has given birth to the concept of "petroleomics" [14–16] to reflect the efficiency of the experimental techniques to map all the crude oils molecules. However, the outcome of this is that the broad majority of molecules will be bulk molecules and as such with a limited interest for the film properties [17]. Such a technique is omitting the propensity of the molecules to form aggregates / nanoaggregates, where the size and the aggregate properties are crucial for the incorporation in the interfacial film [10,18]. Normally the interfacially active amount can be very low, i.e. in the ppm range [17]. For emulsion stabilization it is central how these molecules orient and pack at the interface when building up the films. The first crucial question is whether there is enough interfacially active material to cover the interface of all droplets. It is well-known from film studies based on Langmuir or Langmuir-Blodgett techniques, sometimes coupled with Brewster Angle Microscopy, that the first tendency of the surface-active material such as asphaltenes is to form patches with high local concentrations [19–21]. This has recently been confirmed by microrheology using a new ferromagnetic microbutton techniques [22]. The final film properties are not established before the film pressure is raised. In an emulsion it is of course not possible to mechanically adjust the interfacial pressure, but the same effect is achieved for increased concentration of the surfactant material. Insufficient packing of the crude oil surfactants will leave non-coated parts of the interfaces and increase substantially the probability of coalescence between droplets [23]. Hence factors influencing the coverage is the surfactant concentration, the number of droplets (water cut) and the size of the droplets. In addition to this the temperature will influence the film properties by altering the effective HLB value of the hydrophobic surface-active constituents. In this way their solubility in the oil phase will increase and their interfacial activity will decrease. A natural consequence will be that the composition of the interfacial film will change with temperature. Variations of interfacial film properties (interfacial tension and interfacial rheology) have indeed been observed [24–26].

Another aspect of these films in crude oils systems is that when nanoparticles of asphaltenes are involved there will always be weak parts of the film where the aggregates are integrated into the crude oil film. These sections of the film will have different mechanical properties than the film as an average. When droplets are approaching each other the overlap between droplets will be easier at these sections.

1.1. Outline of the review

This comprehensive review presents the latest findings on the destabilization of crude oil emulsions by electrocoalescence. Both experimental and modelling techniques are discussed and several scales, from the individual droplet to industrial phase separation, are considered. The manuscript is organized according to the scale of the described phenomena starting with the smallest scale, i.e. the oil-water interface, and finishing with the presentation of industrial electrocoalescers.

The effect of electric field on the water-oil interface is discussed in sections 2, which also elaborates the enhancement in adsorption of surface-active components by electric field. The electric field-induced hydrodynamic and kinetic effects at the scale of one droplet are presented in section 3. The coalescence of a drop pair under an electric field is then presented in sections 4 (experimental) and 5 (modelling). The modelling section discusses results obtained by Dissipative Particle Dynamics (DPD) simulations on the formation of pores in the thin film at the onset of coalescence. Finally, the resolution of crude oil emulsions from the bench to the industrial scale is presented in sections 6 and 7. NMR and other selected techniques allowing to follow-up oil-water separation at the bench scale are described.

2. Interfaces under electric fields

2.1. Introduction

The kinetic stability of a multiphase system is determined by the stability of an interface separating two phases locally. For example, in a kinetically stable emulsion the drop interface is stable, which in turn resists the drop-drop approach and coalescence. Multiple factors govern the stability of an interface including surface/interfacial tension, viscoelastic properties, external force fields, etc. The interfacial stability has critical implications in the industrial applications. For example, the shelf life of pharmaceutical, cosmetic and food emulsions/suspensions is dependent on the interfacial stability. In the electrostatic phase separation, drop-drop coalescence is hampered by the phenomena such as partial coalescence [27,28], chain formation [29] and drop breakup [30,31]. In the partial coalescence, when a drop and interface or two distinct size drops coalesce under an electric field, the coalescence might be accompanied by the generation of tiny droplets, much smaller in size than the original drops [27,28] (Section 4.2 presents detailed discussion on the phenomenon). Whereas, the chain formation in an electrocoalescing emulsion refers to the formation of droplet trains oriented in the direction of the external field, where each adjacent droplet is separated by a stable film. Moreover, when the electric stresses dominate the surface tension force, a freestanding drop can distort and disintegrate into several minute progeny droplets [30,31]. All of these phenomena are partly attributed to the interfacial properties and adversely affect the electrostatic phase separation [32].

2.2. Adsorption at liquid-liquid interface in the absence of external forces

The mass transfer and the resultant evolution in the interfacial properties are conventionally modelled using dynamic interfacial tension (IFT), undermining the convections and Marangoni effects. If either phase of a multiphase system contains surfactant, the molecules self-diffuse through the phase to adsorb at the interface separating the phases. The adsorption mechanism can either be diffusion or mixed kinetic-diffusion controlled [33]. In a diffusion-controlled adsorption, after formation of an interface (or after addition of surface active molecules into either phases), the molecules arriving at the empty interface adsorb without diffusing back in to the bulk phase. The rate of adsorption is governed by self-diffusivity of the molecules and the bulk concentration. However, as the interface populates with time, the adsorption can become mixed kinetic-diffusion controlled, where a barrier hinders the arriving molecules from adsorbing [34]. The adsorption barrier can be due to the augmented surface pressure, nearly fully occupied interface or stearic repulsion from the adsorbed molecules [33]. The intermolecular interaction between the adsorbed molecules also contributes to the barrier [35]. The molecules arriving at the interface may diffuse back into the bulk phase if they fail to overcome the barrier. Here the interfacial concentration controls adsorption and desorption dynamics.

The time-dependent interfacial concentration during the diffusion-controlled adsorption can be modelled using the famous Ward and Tordai equation [36]. The model assumes that when the interface is fresh the molecules reaching the interface enter into an imaginary

subsurface and adsorb without resistance. The original model can only be solved numerically; however, its analytical solution was proposed by several workers [37–39] and tested for different surfactants [40–42]. Miller's [43] asymptotic solution gives the short time approximation of Ward and Tordai equation as,

$$\gamma(t) = \gamma_0 - 2nRTC_0\sqrt{\frac{Dt}{\pi}} \quad (1)$$

where γ_0, γ (t), R, T, C_0, D and t denote IFT at $t = 0$, dynamic IFT, gas constant, absolute temperature, bulk concentration, diffusion coefficient and time, respectively. The constant n is 1 for non-ionic surfactants and 2 for ionic surfactants. Eq. (1) can be fitted to time dependent IFT decay to estimate diffusion coefficient at a fresh interface. When the interface becomes more crowded, the probability of the arriving molecules diffusing back into the bulk phase increases. The long-time approximation of the Ward and Tordai equation describes adsorption dynamics as the concentration in the subsurface approaches the bulk concentration. The equation is written as,

$$\gamma(t) = \gamma_{eq} - \frac{nRT\Gamma_{eq}^2}{C_0}\sqrt{\frac{\pi}{4dT}} \quad (2)$$

Here γ_{eq} and Γ_{eq} are equilibrium IFT and equilibrium surface concentration, respectively.

The decay in dynamic interfacial tension as a result of adsorption of surface active molecules can be used to estimate the rate of adsorption and interfacial concentration by fitting a suitable isotherm [33].

2.3. Water-crude oil interface

As mentioned in the introduction section, the crude oil components such as asphaltenes, resins and naphthenic acids are natural surface-active agents [4]. They are water-insoluble and adsorb at water-oil interface, stabilizing the tiny water droplets in crude oil emulsions [44]. Given very small drop size and stable interfaces the crude oil emulsions are challenging to separate. When two water droplets approach each other, the water-oil interface inhibits the film thinning and breakup. Chemical demulsifiers are used in the crude oil industry to destabilize the interface and help the minute droplets coalesce easily to break the emulsified system into water and oil phases. The demulsifier molecules are made of water loving polar parts (hydrophilic) and oil-loving nonpolar parts (hydrophobic). They adsorb at a water-oil interface, with the polar and nonpolar parts oriented towards water and oil respectively, resulting into the reduction in the free energy of the system [45] and making the interface unstable. The chemical demulsifiers (also called chemical dehydrants) are usually the high molecular weight species and if used as emulsifying agents produce oil-in-water emulsions [46]. Thanks to the high diffusivity in crude oils they readily move to adsorb or displace asphaltenes at the interface [47]. The functionality of such chemicals has been a long-lasting debate. A very early suggestion was that they replace the interface consisting of natural components with new interfacial demulsifier components which will give a lower level of stability of the system. However, such an approach can be disqualified based on simple concentration arguments. A demulsifier is normally added in concentrations amounting to 10–50 ppm. If the water cut equals to 30–50 wt% the added interfacial material cannot be enough to cover the existing interfaces with new material. Another versatile approach is that the added demulsifier, which has a documented interfacial activity, is building up a mixed interface together with the indigenous components. Ese et al. [48] proposed that the demulsifier-induced revised viscoelastic properties of the interface replace or displace the adsorbed asphaltenes. To test the mechanism, the rheological properties of demulsifier-modified interfaces were investigated by various groups [49,50]. They found clear indications that an addition of demulsifier modified the elastic / viscous properties of the interfaces in the direction of lost elasticity behavior. With the new mechanical properties, the emulsions lost their stability due to increased coalescence efficiency. Kim and Wasan [51] argued that the reduction in IFT due to the formation of asphaltene-demulsifier complexes destabilizes the interface.

The most commonly used method to develop and test a chemical demulsier for a specific water-in-crude oil emulsion is the bottle test [52]. However, the introduction of electric field-based technique helped to determine the stability of an emulsion quantitatively [52–54]. The method involves application of a linearly increasing steady uniform electric field to a thin emulsion film sandwiched between two parallel metal plates. The electric current flowing through the emulsion is small and constant initially; but shows a sharp increase as the field exceeds a certain magnitude called Critical Electric Field (E_{cr}). For a given emulsion, stable or unstable, the E_{cr} can be constant. Addition of a 'good' demulsifier in an emulsion lowers E_{cr} and the reduction is a function of the demulsifier concentration [54,55]. However, the concentration-E_{cr} relationship is not monotonous; there exists a threshold concentration for each demulsifier above which E_{cr} ceases to drop. The Critical Electric Field method offers a reliable way to compare emulsions for their stability and demulsifiers for effectiveness.

2.4. Interfacial phenomena under electric field

The effect of applied electric fields on the transport phenomena at fluid interfaces has been studied since long. However, due to the absence of appropriate method to monitor dynamic interfacial properties under an electric field, the majority of the studies were limited to theoretical analyses. Axisymmetric drop shape analysis (ADSA) is commonly used to measure the time-dependent characteristics of an interface being adsorbed with surface-active molecules. Such an adsorption may last from a few minutes to hours until the interface is equilibrated. The conventional ADSA algorithms have capabilities to capture and analyze profiles of the interface for a longtime. However, until recently, such an analysis under the electric field was not possible.

The increment in mass and heat transfer at or across a drop interface in an electric field is attributed to the field-induced microflows. According to the leaky dielectric theory, proposed by Sir G. I. Taylor [56], difference in conductivities of the fluids across the interface induces free charge when the electric field is applied. Although the net interfacial charge is zero, given its antisymmetry (the charge on one hemisphere is positive while the other is negatively charged), the charge-field interactions generate fluid flows and toroidal flow patterns appear on the both sides of the interface [57] (demonstrated in Fig. 1). The direction of the circulations- either from poles to equator or equator to poles - is determined by the electrical properties i.e. conductivities (σ) and permittivities (ε) of the both liquids [56–59]. In a static electric field when $\frac{\sigma_m}{\sigma_d}\frac{\epsilon_d}{\epsilon_m} = 1$ no circulations are observed. In the systems with $\frac{\sigma_m}{\sigma_d}\frac{\epsilon_d}{\epsilon_m} > 1$, the flows are directed from the poles to equator, and in the reverse direction when $\frac{\sigma_m}{\sigma_d}\frac{\epsilon_d}{\epsilon_m} < 1$. The circulations are called electrohydrodynamic (EHD) flows and are proved to dampen the heat and mass transfer resistance on the either side of the drop interface.

In a freely suspended stationary drop in an electric field the electrohydrodynamic flows are symmetric about its equator. The symmetry can be shifted away from the equator by tuning the field; which results into stronger mixing inside the drop [59,61,62]. The EHD flow-associated Peclet number (ratio of advective transport and diffusive transport rates) is reported to increase the Nusselt number (ratio of convective and conductive heat transfers) and Sherwood number (ratio of convective mass transfer rate and diffusion rate). However, there is an unanimity among the most theoretical studies that in a fluid system a maximum steady state Nusselt or Sherwood number is reached and the further increase in Peclet number is ineffective [63–67]. Our recent experimental observations substantiated the theoretical results, where we found that increasing the electric field strength (thus the EHD flow intensity and Peclet number) to a certain limit increases the adsorption

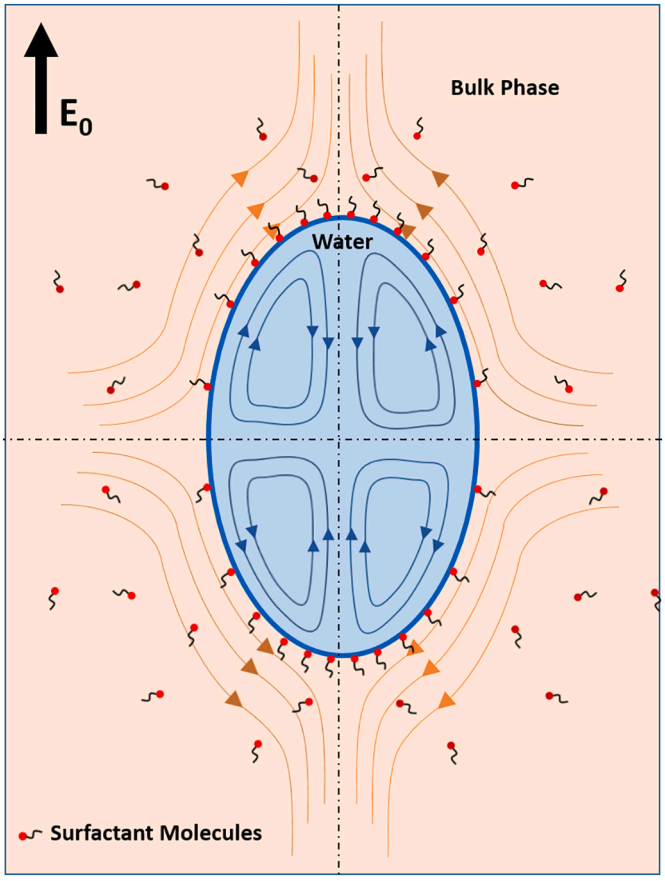

Fig. 1. Schematics of the electric field-induced axisymmetric flow circulations and adsorption at a water-oil interface. Reproduced from Mhatre et al. [60] with permission from the American Chemical Society.

and interfacial concentration [60].

The theoretical studies followed different approaches; some assumed the heat/mass transfer resistance on bulk side of the interface ('the external problem'), while the other considered it lies inside the drop ('the internal problem'). Morrison [63] and Griffiths et al. [64] in their 'external problem' studies observed that the heat and mass transfer are independent of the EHD flow directions. Another important finding includes the magnified transfer rates increase further if the drop is translating [65,66]. Jog and group [68–71] addressed the stationary as well as translating drops in the static and periodic electric fields. In each individual case the transport rates are governed by the applied field-attributes such as strength, homogeneity, frequency, etc. Their numerical analysis showed similar effects of electric field on mass and heat transport as reported by the previous studies. Contrarily Chang et al. [72] ruled out any effect of the applied field on mass and heat transfer in their study on the relative contribution of gravity and the electric field-induced flows.

Several experimental studies reported observations indicative of the effects of applied electric fields on interfacial phenomena [73–76]. However, majority of the studies lacked systematic measurements and interpretation of the observations. Schmid et al. [77] and Hurd et al. [78] used surface energy balance to measure surface tension of aqueous salt solutions under strong electric fields. They ascribed a significant reduction in the surface tension under electric field to the rise in interfacial charge density. However, the results could not be validated with a thermodynamic analysis by Hayes [79]. Given unreliability of the surface energy balance method, the reported reduction in the surface tension in strong DC electric field is far-fetched.

A liquid drop, surrounded by another miscible liquid and exposed to an electric field, undergoes stretching in the direction of the field. If the interfacial tension is time dependent (due to the presence of surface-active molecules), the stretching magnifies with time. Kotaka and group [80–83] reported the similar shape deformation of a pendent drop due to the applied field in several surfactant-rich solutions. Degen et al. [84] used the deformation behavior of pendent water drops and capsules to investigate mechanical properties of the interfaces. Similar to the pendent drops, the electrowetting behavior of sessile drops in the presence of surfactants has been extensively studied. In a series of reports Counce and group [85,86] demonstrated the influence of the electric field on the contact angle of a drop on metal surfaces. Majority of their studies were performed in a highly asymmetric electric field generated by a pin-plate electrode system, where the voltage was supplied to the metal surface and the pin was grounded. In an attempt to demonstrate relationship between the applied field and adsorption, Santiago et al. [86] measured contact angle of a sessile phenylmethyl polysiloxane droplet on a stainless steel plate. The drop was surrounded by aqueous SDS solution and the applied voltages and its range was small, −3 to 3 V. They reported a significant change in the contact angle; however, failed to explain mechanism of the contact angle reduction and its non-linear dependence on the applied field.

A pendent drop surrounded by a surfactant-rich medium exhibits a time-dependent shape deformation in the direction of gravity. When the system is put into an electric field, directed parallel to gravity, the deformation amplifies [80,84]; which is obvious as a drop in an electric field distorts in the direction the field. When the field is horizontal, interestingly, the drop continues stretching in the vertical direction [87]. In our investigation of the shape of a pendent water drop held in an organic phase containing asphaltenes we observed that the drop microscopically deformed with time. The adsorption of asphaltenes and resultant decay in the interfacial tension were responsible for the temporal deformation of the drop. When a DC electric field was applied to the drop in the horizontal direction, the drop showed a momentary deformation in the field direction; however, the deformation quickly subsided and the drop started stretching vertically attaining a steady shape. The temporal as well as equilibrium vertical deformations were found to be governed by the bulk concentration and the applied field strength. The counter-intuitive shape change and its magnification with the applied field suggested the intensified adsorption dynamics at the water-oil interface.

A systematic experimental attempt to show the influence of electric forces on mass transfer at liquid interfaces had been limited until recently. The absence of accurate method to measure the interfacial properties under an electric field was the primary reason. Axisymmetric drop shape analysis (ADSA), a drop profile-based technique, is a commonly used method to monitor dynamic interfacial tension over a long time. The method involves holding a sessile or pendent drop in a bulk phase and continuously capturing the drop images. An experimentally obtained drop profile is iteratively fitted to a theoretical drop profile, generated using the Young-Laplace equation, by updating the gravitational Bond number, $B_0 = \frac{R_a^2 \Delta\rho g}{\gamma}$. Here R_a is the radius of curvature at drop's apex, $\Delta\rho$ is density difference between drop and surrounding fluids and g is gravity constant. The interfacial tension (γ) is calculated from B_0 at the optimum fit between the two profiles. The method is fairly accurate in the absence of external force fields. However, when a clean drop is exposed to an electric field, the conventional ADSA algorithms result into γ linearly decreasing with the field strength [88]. Similar reduction in water-xylene interfacial tension under DC uniform electric fields, estimated using the ADSA method, is presented in Fig. 2. Such a reduction in interfacial tension in the absence of surface-active molecules is unwarranted.

When the conventional Young-Laplace equation is used to estimate interfacial tension under an electric field the Maxwell stresses at the drop interface are disregarded, which leads to the inaccurate γ values. In order to apply ADSA to a drop under an electric field and to

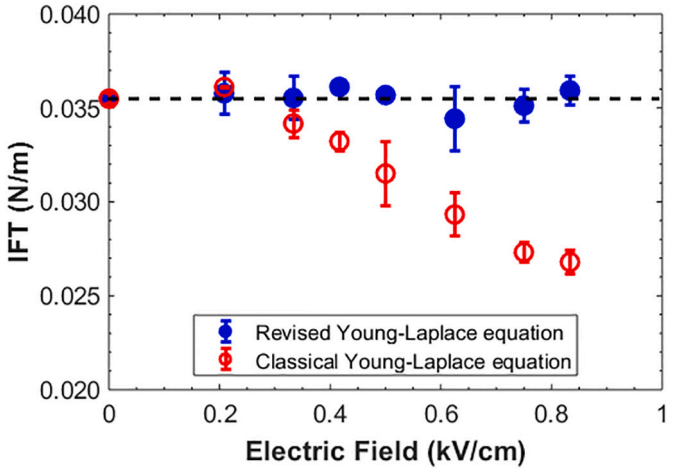

Fig. 2. Interfacial tension of water-xylene interface under electric field, calculated using conventional and augmented ADSA algorithms. Reproduced from Mhatre et al. [88] with permission.

systematically investigate the field-effect on mass transfer at the drop interface, we revised the Young-Laplace equation to include Maxwell stresses [88]. The electric field at the interface was calculated with finite difference method. The ADSA algorithm could process a large number of experimental drop images to return corresponding interfacial tension. The method was validated with a pendent water drop in xylene under a DC electric field. The water-xylene interfacial tension calculated by using the updated ADSA algorithm was found constant irrespective of magnitude of the applied electric field (demonstrated in Fig. 2).

The electric field-based ADSA algorithm made possible a careful investigation and analysis of adsorption dynamics under electric field. Our work on a pendent water drop held in an asphaltene rich organic phase subjected to a uniform DC electric field [60] validated the previous theoretical results. The two subfractions of asphaltenes used in the study- irreversibly adsorbed (IA) and bulk asphaltenes- exhibited electric field dependent adsorption behavior. The dynamic and equilibrium interfacial tension were observed to significantly decrease with increasing the field strength (Fig. 3). The diffusion-controlled adsorption mechanism quickly turns to the mixed diffusion-kinetic after application of the electric field, suggesting an early crowding of the interface. The adsorption was observed to be irreversible as the equilibrium IFT (γ_{eq}) attained under the electric field remained unchanged after the field was switched off. Furthermore, the diffusion coefficient and equilibrium surface concentrations were turned out to be higher under the stronger fields. The bulk asphaltenes had weaker affinity to water-oil interface; however, the degree of γ_{eq} reduction and increase in diffusion coefficient were found to be higher in comparison with IA asphaltenes.

The scaling of the γ_{eq} data for the both asphaltene subfractions suggested that the abovementioned effects were independent of the bulk concentrations and can only be attributed to the electrohydrodynamic flows [60]. However, the mass transfer enhancement reached a steady state when the electric field exceeded a limit; which was in agreement with the previous theoretical findings that the Nusselt and Sherwood numbers stop increasing if the Peclet number is increased beyond a threshold. We found that the threshold was surfactant-specific, it was distinct for IA and bulk asphaltenes.

The majority of above-mentioned studies in the literature, with and without electric fields, involved single surface-active species. The phenomena of interplay between different surface-active crude oil components and their adsorption at water-oil interface, when exposed to an electric field, still remain unexplained. Therefore, to further boost the phase separation capabilities of the electrocoalescence method, understanding the phenomena, its influence on the properties of the interfaces and consequently its role in film thinning and film rupture stages of drop-drop coalescence are crucial.

3. Drop electrohydrodynamics

3.1. Drop shape and stability

A liquid drop's response to an externally applied electric field has been studied for a century now. The first detailed scientific investigation is credited to Zeleny [89] who observed the electric field-induced disintegration of a water drop suspended from a capillary. In 1924 Melvin Mooney [90] did the systematic experiments on the mobility of oil drops in aqueous media under low strength DC electric fields. Similarly, Nolan's [91] experiments showed drop instability and breakup as a result of the applied electric fields. The initial studies on the drop

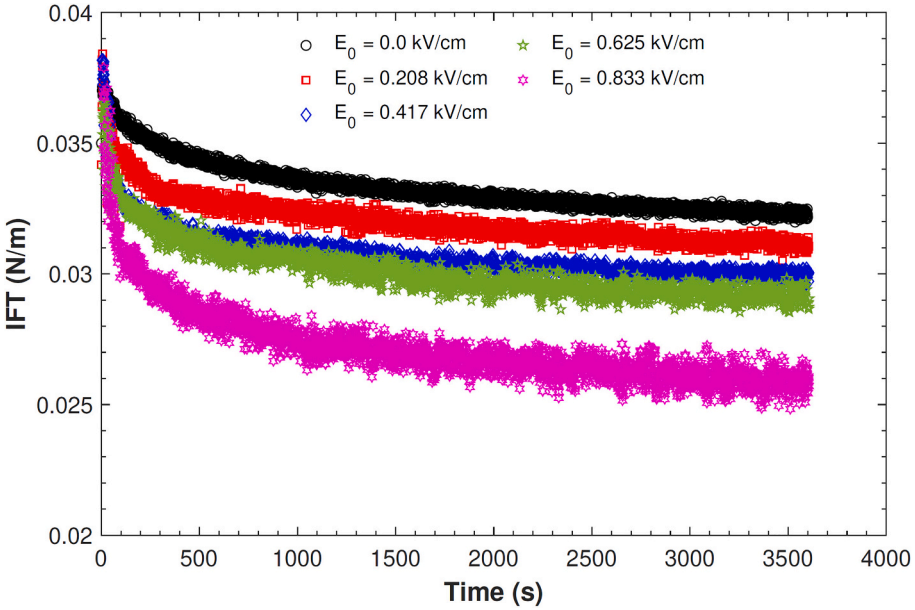

Fig. 3. Dynamic IFT of pendent water drop in xylene interface under various DC electric field strengths when the bulk phase contained 0.05 mM of irreversibly adsorbed asphaltenes. Reproduced from Mhatre et al. [60] with permission from the American Chemical Society.

electrohydrodynamics, interplay between electrostatics and hydrodynamics, were primarily aimed to understand natural phenomena of raindrop breakup in the thunderstorms [92]. However, the recent developments in the drop electrohydrodynamics are inspired from a range of modern scientific applications including ion mass spectroscopy, inkjet printing, droplet-based microfluidics, etc.

When a neutrally buoyant liquid drop surrounded by another immiscible liquid and exposed to an electric field (E), the difference in electrical properties of the two fluids induces electric stresses at the drop interface. The initially spherical drop assumes a new shape which is defined by the equilibrium between capillary, hydrodynamic and electric stresses. When the electric stresses overpower the stabilizing surface tension force, the instability sets in and the drop disintegrates. Zeleny [89] attributed the drop breakup to hydrodynamic instabilities which was later refuted by Taylor [93]. When the medium phase is a perfect dielectric the normal electric stresses at the drop interface are balanced by the updated capillary pressure due to the shape deformation [94]. Whereas, when the medium is more conducting, the tangential electric stresses at the drop interface generate flows on either sides of the interface [56].

In a fluid system consisting of a drop phase more conducting than the medium, e.g. water drop in oil, the drop assumes prolate spheroidal shape when put into a uniform steady electric field. Its polar length increases with strength of the electric field and reaches limiting length 1.9 times the equatorial length before it starts disintegrating [93]. The electric stress at the poles amplifies as the length increases. Whereas, when the surrounding phase is more conducting, the drop compresses along the field direction and acquires an oblate shape. In the either cases the drop shape does not lose symmetry.

The electric conductivity ($R = \frac{\sigma_m}{\sigma_d}$) and permittivity ($Q = \frac{\epsilon_d}{\epsilon_m}$) ratios determine shape of a freely suspending uncharged drop in an electric field. Here σ and ϵ denote electrical conductivity and permittivity, respectively; while subscripts d and m indicate drop and medium phases, respectively. The induced electrohydrodynamic (EHD) flows and resultant drop deformation, determined by the electric property ratios, are demonstrated in Fig. 4. When RQ = 1, the surface charged density (σ_s) at the drop surface is zero, the electric field does not induce flows on either sides of the interface and the drop retains its spherical shape [58]. In the fluid systems with RQ < 1, the drop hemisphere oriented towards the positive electrode acquires negative charge, the EHD flows are directed from the equator to the poles and the drop attains a prolate shape. The polarity and the flow direction are reversed if RQ > 1 and the resultant drop shape is oblate. The criteria for EHD flow patterns and drop deformation apply to steady as well as alternating electric fields. When the field is oscillating the frequency is an additional parameter that controls the flow fields [58,59]. However, the EHD flows, polarization and deformation of the drop are independent of the polarity of voltage supply as the other electrode always acts as a counter electrode with opposite polarity induced surface charge.

A strong electric field breaks a drop in two distinct ways, namely electric and electrohydrodynamic breakups [58]. The electric breakup is attributed to the electric stresses and the electrohydrodynamic breakup to both the electric and hydrodynamic stresses. Dubash and Mestel [95,96] reported that at an electric field below critical strength (E_C) the drop exhibits spheroidal deformations. The critical field strength corresponds to the field at which drop loses stability. The resultant equilibrium shape is independent of viscosities of the either phases. However, the time of drop deformation and breakup is determined by the viscosity ratio ($M = \frac{\mu_d}{\mu_m}$) and the field strength (E) [80,96], where μ_d and μ_m are viscosities of drop and bulk phase, respectively. When E exceed E_C the drop breaks through different modes [95] depending on M and E. The breakup modes include (a) lobe formation and breakup at the stretched drop's polar ends (shown in Fig. 5.a), (b) polar ends acquire conical shape which ejects thin jet (Fig. 5.b), and (c) jet ejection from obtuse polar ends. When R and M are very small the drop stretches to a rod shape and breaks with bulbous ends. *Ha* and Yang [97] reported this mode of breakup at R < $O(10^{-6})$ and M $O(10-3)$. Increase in R and M (O

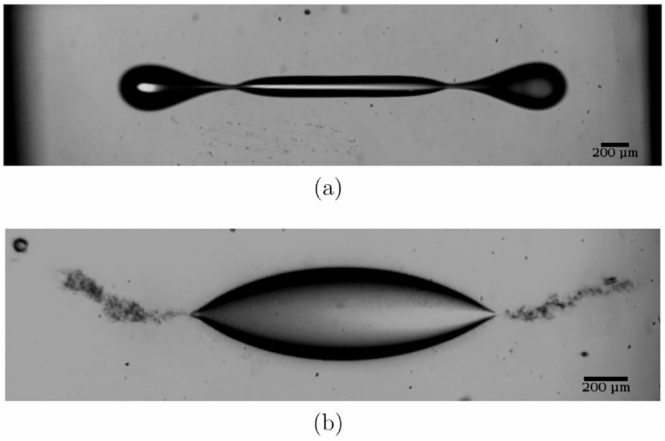

Fig. 5. a) Water droplet breakup by bulbous ends when surrounded by a pure oil and subjected to a strong uniform DC electric field. (b) Tip streaming breakup of an octadecyltrichlorosilane (OTS)-covered water drop (after Karyappa and Thaokar [98]). Reproduced with permission from the American Chemical Society.

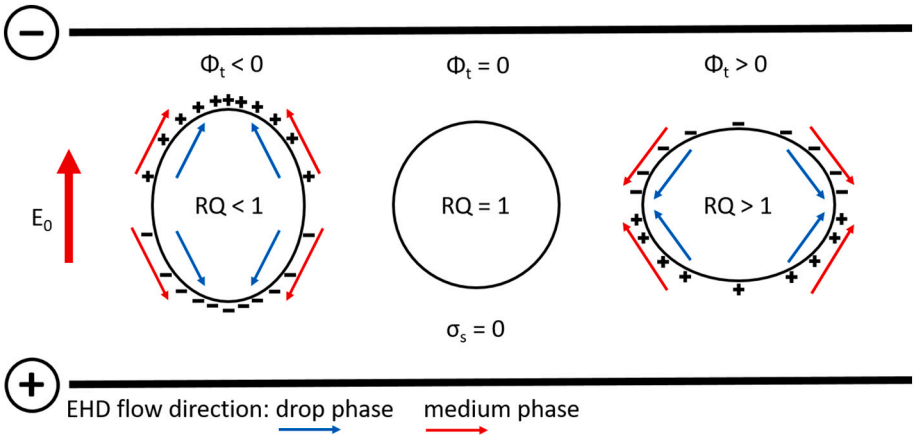

Fig. 4. Schematic presentation of induced charge distribution, drop deformation and direction of EHD flows in drop and medium phases under uniform electric field. The surface charge density $\sigma_s = 0$ and tangential component of electric stress, $\Phi_t = 0$ when RQ = 1. EHD flows are directed from the equator to the poles and drop assumes prolate shape when RQ < 1; while flows are in the reverse direction and the drop deforms to oblate shape if RQ > 1. (redrawn from Torza et al. [58]).

(1)) turns the breakup mode to the jets ejecting pointed ends, where the equatorial part holds most of the liquid volume. This mode is more likely when the both phases are non-Newtonian.

The drop breakup can be catastrophic and introduce a large number of daughter droplets into the surrounding phase. In their systematic experimental study Karyappa et al. [31]. reported that the drop breakup is a strong function of viscosity ratio as well as electric capillary number. The electric capillary number, $Ca_E = \frac{\varepsilon_m a E^2}{\gamma}$ is the ratio of electric and capillary stresses acting at the drop interface.

Ha and Yang [97] carried out extensive experimental studies on effect of the rheological properties of the phases on drop stability and breakup. They observed that the non-Newtonian properties of either phases do not influence the drop deformation; however, their effects on critical conditions of breakup and breakup modes are noticeable. At $M > 1$, a drop is more stable if drop phase elasticity is larger (than medium phase elasticity) whereas it easily loses stability when the medium phase is more elastic. Opposite effects can be observed at $M << 1$.

The shape of the spheroidal drop is conventionally expressed as degree of deformation, $D = \frac{L-B}{L+B}$, where L and B are its polar and equatorial diameters, respectively. Taylor's small deformation theory gives relationship between the equilibrium degree of deformation and the strength of applied electric field when the deformation is limited [56].

$$D = \frac{9}{16(2R+1)^2} Ca_E \left[\left(1 + R^2 - 2SR^2\right) + 3R(1 - SR)\frac{2+3M}{5+5M} \right] \tag{3}$$

When the drop phase is perfectly conducting, Eq. (3) reduces to $D = \frac{9}{16} Ca_E$. The expression for the degree of deformation is valid when the both drop and medium phases are Newtonian.

Drop's mobility in an external field is determined by the field configuration. As discussed above, in a uniform electric field a drop can translate if it bears net charge (electrophoresis) or remains standstill if it is uncharged. An uncharged drop polarizes when put in to a uniform electric field; where the induced charges are distributed antisymmetrically. Therefore, as the net force on the drop is zero, it remains stationary. Whereas, an asymmetric non-uniform field sets a drop in motion regardless of charge. Different other kinds of field configurations have also been used to investigate drop behavior. A drop placed in a symmetric non-uniform field generated by quadrupolar electrode setup does not move which makes easier to study its shape and stability [99,100].

The breakup of a liquid drop, at Ca_E above a critical limit, leads to the generation of progeny droplets much smaller in size than the original drop. The phenomenon can be employed as an emulsification method to generate nearly monodispersed emulsions, where the strength and the time of field application determine characteristics of the resultant emulsion [101,102]. Different modes of the drop disintegration can be observed depending on electrical conductivity (R), permittivity (Q) and viscosity (M) ratios [31,97]. However, in an electrocoalescing emulsion the drop breakup adversely affects the rate of coalescence. The breakup at a very large electric capillary number introduces minute droplets in the emulsion bringing down the average droplet size instead of increasing. Therefore, identifying the critical capillary number for an emulsion and operating phase separators below the critical field strengths is crucial in industrial operations.

3.2. Electrophoresis and dielectrophoresis

In the electrostatic demulsification, in addition to the dipolar forces, electrophretic and dielectrophoretic forces significantly influence drop mobility and coalescence probability. The droplets can be inherently charged due to the ionic adsorption at the interface. However, in the non-ionic systems droplets can acquire net charge through contact charging at electrode surface. The amount of charge acquired by a drop of radius a is expressed as, $Q_c \propto a^u E^v$. The exponents u and v are given by the field configuration; they are reported to be different in uniform [103,104] and nonuniform electric fields [105]. The electrophoretic force ($F_e = Q_C E$) propels the droplet towards the electrode of opposite polarity. During the translation, it comes into contact with uncharged droplets and merges.

An uncharged drop (or solid/bio particle) placed in a non-uniform electric field experiences net force which sets the drop in motion. The phenomenon is called dielectrophoresis and it exists in a majority of scientific and industrial applications as the local field around a drop loses uniformity due to a variety of reasons. The dielectrophoretic force is defined as [106],

$$F_{DEP} = 2\pi a^3 \varepsilon_m f_{CM} \nabla E^2 \tag{4}$$

The Claussius-Mossotti factor, $f_{CM} = \frac{\varepsilon_d - \varepsilon_m}{\varepsilon_d + 2\varepsilon_m}$, determines which direction the drop would be driven. When f_{CM} is positive, the drop is attracted to the stronger electric field region, which is called Positive Dielectrophoresis and reverse if f_{CM} is negative (called Negative Dielectrophoresis).

The diectrophoresis in an emulsion leads to a range of phenomena which may help or hamper the coalescence process. The F_{DEP}-induced motion and segregation increase probability of the drop-drop contact and positively affect the coalescence rate [107]. If a migrated drop comes into contact with an electrode, it acquires net charge and moves away from the electrode. The drop undergoes periodic motion as result of equilibrium between dielectrophoretic, electrophoretic and drag forces [104,105,108]. The periodic motion contributes to the convection near electrode surface which assists in the drop contact. However, in the systems involving poorly conducting fluids, positive dielectrophoresis leads to the breakup of droplets arrived at the electrode surface [101]. The size of the resultant droplets can be significantly small, reducing average drop size of the emulsion and consequently reversing the rate of electrocoalescence.

A dielectrophoretically translating drop experiences chaotic flows on either sides of the interface [109]. The EHD flows in drop phase generate flow patterns at the interface, enhancing mass transfer dynamics. The non-axisymmetry of the background electric field breaks the symmetry of flow patterns otherwise seen under uniform fields. Similarly, the drop shape loses symmetry as the electric field gradient increases and it approaches an electrode. In highly asymmetric fields, the conducting droplets are observed to acquire a pearl shape when close to the strong field electrode. The pointed end is oriented in the electrode direction; which grows into a thin unstable jet if the field is increased above a critical limit.

3.3. Pickering/particle-stabilized drops

There are quite a few studies on electric field induced patterning of colloidal particles at a drop interface. Electric fields can be effectively used to segregate and maneuver the colloidal particles at liquid interfaces [110]. The naturally occurring particles in crude oil such as silica, clay, etc. contribute to the stability of crude oil emulsion [111–113]. The water-oil interface stabilized with the particles and asphaltenes together is more stable than it is stabilized by asphaltenes alone [114]. Nudurupati et al. [115] proposed employing the drop-breakup modes (mentioned in the previous subsection) to strip off colloidal particles adsorbed at a drop interface. In the multiphase systems with $RQ < 1$, EHD flows from drop's equator to the poles carry and accumulate the particles at the poles. Application of strong electric fields results into formation of conical tips that eject particle-concentrated tiny droplets in to the bulk phase. When $RQ > 1$ the interfacial particles segregate along the equator. Stretching the droplet and breaking it in to a number smaller droplets produce the particle-rich progeny droplets in the centre. Although smaller in size, the newly generated droplets sediment faster due to larger densities. Similarly, a non-uniform electric field can be used for interfacial sorting and segregation of particles having distinct electrical properties. In this case the particles having positive and negative f_{CM} accumulate at opposite poles of a droplet

[116]. The particles can be selectively separated from the drop phase by further increasing the field.

4. Drop-drop electrocoalescence

4.1. Coalescence mechanism

In an emulsion the coalescence of individual droplets and growth in average drop size are preliminary steps towards phase separation. The increased droplet size speeds up gravity settling and development of a liquid layer at bottom. The coalescence of a pair of droplets occurs in three steps; namely (i) drop-drop approach, (ii) film drainage and (iii) thin film breakup [117]. Two adjacent droplets approach each other under the influence of external force(s) or gravity and as they are very close a film of the medium fluid separating them squeezes out. At the end of the thinning, a film between the droplets ruptures allowing them to mix. When the emulsion is placed into an electric field, each of the stages are individually influenced by the field.

The attraction between adjacent droplets is largely attributed to the dipolar drop-drop interaction induced by the applied electric field. Each drop is polarized with antisymmetric charges at its surface and the attraction between nearest opposite polarity poles pulls the droplets closer. The droplets assume a spheroidal shape as demonstrated in Fig. 6, which is also discussed in Section 3 Drop Electrohydrodynamics. The radial and tangential components of the force of attraction between a pair of droplets are expressed as [30,118]:

$$F_r = -12\pi\varepsilon_m b^3 E_0^2 \left(\frac{a^3}{d^4}\right)\left(3Mcos^2\theta - 1\right) \tag{5}$$

$$F_\Theta = -12\pi\varepsilon_m b^3 E_0^2 \left(\frac{a^3}{d^4}\right) Nsin2\theta \tag{6}$$

a and b represent the undeformed drop radii, s_0 and d the initial surface-surface and centre-centre separations, and Θ the angle between applied electric field and the line joining drop centres. When the droplets are far such that the minimum surface-surface distance s is larger than the smaller drop radius i.e. $s >> b$, each droplet acts as a dipole where $M = N = 1$. Whereas, when the drops come closer and $s < b$, an accurate estimate of the attractive force due to the mutual induction of dipoles between two droplets is given by Eqs. (5) and (6) with $M = 1 + \frac{a^3 d^5}{\left(d^2-b^2\right)^4} + \frac{b^3 d^5}{\left(d^2-a^2\right)^4} + \frac{3a^3b^3\left(3d^2-a^2-b^2\right)}{\left(d^2-a^2-b^2\right)^4}$ and $N = 1 + \frac{a^3 d^3}{2\left(d^2-b^2\right)^3} + \frac{b^3 s^3}{2\left(d^2-a^2\right)^3} + \frac{3a^3b^3}{\left(d^2-a^2-b^2\right)^3}$. The equations suggest that a pair of free drops do not interact unless $54.71 > \theta > 125.19$; which is in agreement with experiments irrespective of physical and electrical properties of the fluids [30].

Other electrohydrodynamic phenomena, including electrophoresis and dielectrophoresis, also increase the probability of drop-drop contact. If a drop bears net charge, the applied electric field drives it towards the opposite polarity electrode. The contact with oppositely charged or uncharged droplets on the way leads to coalescence. However, given finite conductivity of the medium phase the drop loses the charge quickly and does not migrate far. Therefore, the effect of electrophoresis is limited to the region next to an electrode surface where droplets continuously acquire charge through contact charging. Whereas, the dielectrophoretic motion of droplets exist only if the applied field is divergent where the droplets need not be charged. The non-uniformity of the local field could be due to the geometry of electrodes or presence of droplets in the vicinity [107]. The droplets segregate either in strong or weak field- strength region depending on Claussius-Mossotti factor, $\frac{\varepsilon_d-\varepsilon_m}{\varepsilon_d+2\varepsilon_m}$ [105,108]. The induced motion and drop segregation reduce the inter-drop distance and increase probability of coalescence.

For a pair of charged or uncharged drops, the coalescence or retreat without coalescence is determined by the curvature of bridge the drops form upon their contact [119]. If the half angle of the neck, formed at the contact of conical tips at leading faces of the drops, exceeds 31° the drops recoil before the coalescence completes. Bird et al. [119] suggested that the curvature is governed by electric capillary number Ca_E which was confirmed by the numerical calculations by Roy and Thaokar [120]. However, recent experimental studies reported its dependence on electrical conductivity of the drop phase [121–124].

Two charged drops of conducting fluids do not coalesce when subjected to strong DC electric fields, instead the large charge density leads to bursts at inner poles of the drops [125]. Hasib and Thaokar's[124] experiments, involving electrified anchored drops, demonstrated the influence of drop phase conductivity on coalescence modes: non-coalescence, coalescence and partial coalescence. The conductivity was observed to be responsible for the coalescence behavior; however, it was markedly different when the medium phases were air and oil. The authors attributed the difference to the absence of viscous stresses in drop-in-air case; however, more systematic studies on the combined role of viscosity and conductivity ratios in coalescence and suppression of partial coalescence of freely suspended uncharged drop pairs are crucial.

4.2. Partial coalescence

A drop falling through a medium phase, against an interface with the bulk containing same fluid as the drop, straddles before film thinning and rupture. The time for drop's merging with the lower bulk phase depends on drop size, velocity, interfacial tension as well as densities and viscosities of the two phases. The coalescence may be followed by ejection of smaller secondary droplets into the medium phase which eventually fall back and merge to the lower phase [126–128]. Following four dimensionless numbers govern the partial coalescence phenomena in the absence of external force fields [129–132]; the Ohnesorge number

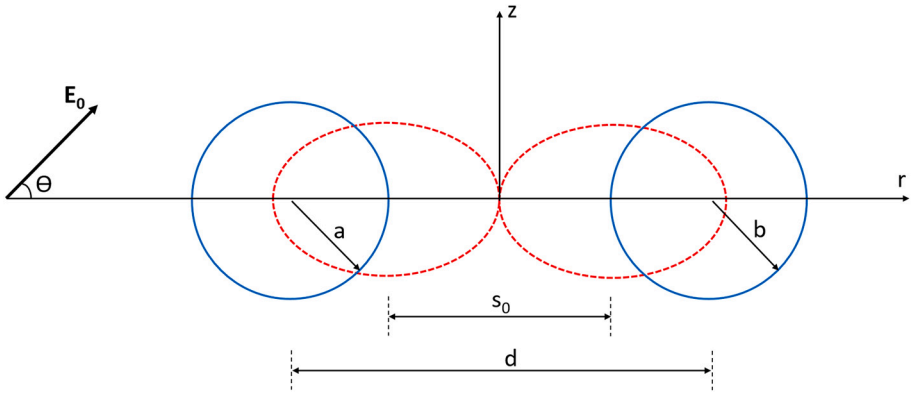

Fig. 6. Schematic of drop-drop attraction in an electric field. Initially spherical drops (blue) deform into spheroidal shapes (dashed red) and move closer after electric field (E_0) is switched on.

$Oh = \frac{\mu_d}{\sqrt{2(\rho_d+\rho_m)\gamma a}}$, the Bond number $B_0 = \frac{4ga^2(\rho_d-\rho_m)}{\gamma}$, density ratio $\frac{\rho_d}{\rho_m}$ and viscosity ratio $\frac{\mu_d}{\mu_m}$. In the higher *Oh* number fluid systems, stronger viscous forces aid the complete coalescence. The drop-interface interaction resembles the coalescence of distinct size drop pairs as well as sinking of the settling drops into a free water layer at the bottom of a coalescing emulsion.

In the electrostatic phase separation, the partial coalescence is considered an adverse phenomenon as it may introduce tiny daughter droplets in the emulsion and hamper the rate of phase separation. The presence of the electric fields and/or interfacial charge may contribute to the effect. Kavepour and group [133] first demonstrated the partial coalescence under an electric field and a flurry of articles reporting high speed photography of the phenomenon followed. The presence of an electric field raises the probability of secondary drop formation and its size [28,133]. The drainage time before the drop merges into liquid interface reduces upon increasing the applied field strength [134]. Hamlin et al. [135] demonstrated that the higher conductivity of drop phase suppresses the partial coalescence when the coalescing interfaces are oppositely charged. Akin to the uncharged drop coalescence, capillary pressure determines size of the secondary droplets as well as its net charge.

When the electric field strength exceeds a threshold, the drop-interface coalescence may be followed by ejection of a jet and spraying of minute droplets in the medium phase [136]. A liquid column emerging after a complete coalescence or a simple partial coalescence - involving generation of a secondary drop, its cascade motion and eventual disappearance - undergoes the electric field induced axisymmetric and whipping instabilities [137] (as demonstrated in Fig. 7). For a column with radius δ, the threshold is determined by the electrical pressure per unit length of the jet $E_0^2(\varepsilon_d - \varepsilon_m)$ and the surface tension pressure per unit length $\frac{2\pi\gamma}{\delta}$. When the former exceeds latter, Rayleigh instability of the jet is suppressed and the column ejects a stream of tiny droplets. The stability of the jets is determined by the field strength and independent of conductivity and viscosity.

Another phenomenon, involving retreat of about-to-coalesce drops followed by the bridge breakup, introduces smaller droplets into an electrocoalescing emulsion. It occurs predominantly during the coalescence of highly dissimilar sized drops under strong electric fields [138]. When the uncharged drops approach towards each other, the strong field between facing poles and electrostatic pressure at the interface quickly squeeze and break the thin film separating the poles. The bridge formed between the drops allows redistribution of the polar charge and thus the electrostatic pressure. If the drop phase is conducting and the applied field is strong, the large charge density at the smaller drop's outer pole pulls the drop away, ceasing the coalescence. The bridge may stretch and break into a string of tiny droplets followed by spraying from conical tip on the drop's inner pole [30]. Hellesø et al. [139] observed similar breakup during coalescence of two charged drops surrounded by crude oil at high temperature.

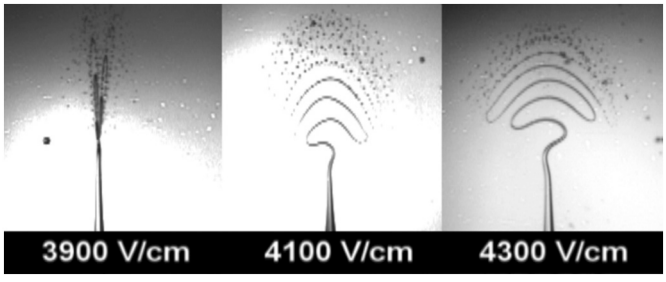

Fig. 7. Electrospraying and electrospinning during partial coalescence of a glycerol drop with silicon oil-glycerol interface. The applied field is perpendicular to the interface with high voltage electrode in contact with silicon oil and ground electrode submerged in glycerol. An instability after the drop ingested into the interface brings about a jet of glycerol emerging from its bulk at bottom (after Aryafar and Kavehpour [136]). Reproduced with permission.

4.3. Coalescence of stable drops

The presence of surfactants at the coalescing interfaces induces additional resistive force due to disjoining pressure from the tail-tail interaction [140]. The disjoining pressure goes on increasing upon increasing the surfactant concentration, leading to the altered coalescence conditions under electric field.

The systematic fundamental studied on binary drop coalescence in crude oil systems are challenging due to difficulties in visualization. Although a near-infrared (NIR) camera can be used to capture the coalescence in asphaltenic phases [139], its use in the electrocoalescence literature is scarce. The majority of drop-drop electrocoalescence studies in the literature are done using vegetable or mineral oils as medium phase. Given the distinctly different physical properties of water-crude oil interface, the reported studies do not accurately represent the coalescence in crude oil emulsions. The variety of natural components of crude oil are adsorbed to the interface and impart peculiar mechanical properties to it. The polar components such as asphaltenes and resins as well as non-polar components such as clays contribute to the interfacial properties, which are impossible to mimic in the vegetable or mineral oil systems.

In our recent work we could demonstrate that the electrocoalescence behavior of stabilized interfaces indeed differs from that of the clean interfaces [141]. We used asphaltenes as well as commercial chemical demulsifiers to cover the interfaces of pendent brine drops. Being the most polar component of crude oil, asphaltenes are primarily responsible for stability of the water-oil interface. A method was developed to stabilize and enable capturing the interaction between the drop pair, where the interface is allowed to age in an asphaltene solution and the dark solution is replaced with a clear solvent until the drops are visible to a camera.

A pair of the anchor drops may remain standstill, attract or coalesce depending on applied DC potential difference and separation as demonstrated in Fig. 8. If the potential difference between the two drops (ΔV_0) is low the Coloumbic attraction is weak to induce any visible interaction. However, if ΔV_0 is increased above a threshold ΔV_m the drops lean inward reducing inter-drop separation [141]. The reduction is instantaneous and constant, scale of which is directly proportional to ΔV_0. Above a critical strength $\Delta V_0 \geq \Delta V_{crit}$ the drops exhibit spontaneous coalescence.

We elaborately studied the effects of differently stabilized interfaces on ΔV_m, ΔV_{crit} and degree of the attraction at potentials in between. Counterintuitively the presence of the surface-active compounds at the drops' interfaces were observed to lower ΔV_m and ΔV_{crit}. In the case of asphaltene-stabilized drops, the thresholds were lower in comparison with the clean drop pair and the further reduction was observed upon aging the drops into more concentrated solutions. The drops populated with commercial chemical demulsifiers showed similar effects. Clearly the interfacial properties dictate various aspects of the coalescence dynamics regardless of the external force fields. In the absence of an electric field two stable drops do not coalescence unless pressed hard against each other. However, the same pair of drops may merge at lower electric field than the drops without surface active molecules at their interface.

5. DPD modelling of coalescence in electric fields

5.1. The coalescence mechanism without electric fields and DPD simulations

5.1.1. The coalescence mechanism

The macroscopic concepts of coalescence have already been presented in Section 4.1. In this section, we focus on the microscopic

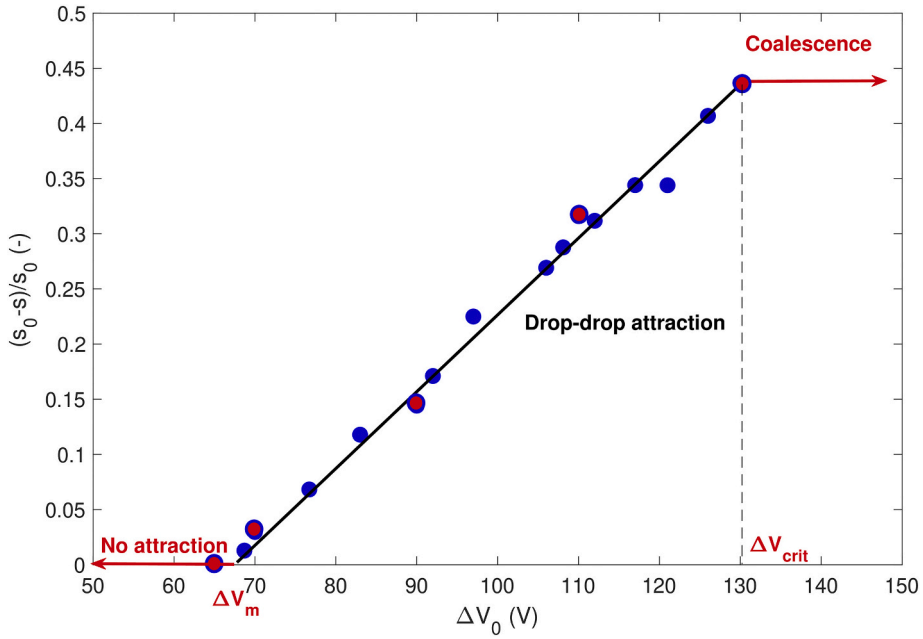

Fig. 8. Interaction between a closely spaced pair of electrified anchored drops. The minimum separation between drops' interfaces s reduces from the initial separation s_0 after potential difference ΔV_0 is applied (after Mhatre et al. [141]). Reproduced with permission from the American Chemical Society.

processes on the molecular scale, and cover some aspects occurring in the thin oil film separating water droplets during the coalescence. A molecular simulation approach has been used to gain more insights into the kinetic aspects. In addition, an electroporation approach, originally developed for cell membranes, has been used to analyze the interfacial energies that have to be overcome in coalescence process.

The essential component in a coalescence event between two emulsion droplets is the process of reconnecting fluid domains in the presence of thin layers of interfacially active molecules. In the case of surfactant stabilized water-in-oil emulsions, one would have two water domains separated by a thin semi-lamellar oil layer with surfactant layers at both oil-water interfaces. In the limit of vanishing oil film, just prior to the coalescence event, only a surfactant bilayer between the water droplets remains. The hydrocarbon tails, or more generally the hydrophobic part of the interfacially active molecule, interacts favorably in the interior of the bilayer, representing a cohesive energy that has to be overcome for the bilayer to open up. Coalescence can only occur if the initial pore opening is unstable and expands to large radius compared to the thickness of the bilayer [142,143]. The energy barrier or line tension associated to the opening of a pore can provide significant emulsion stability.

More complex surfactant systems would not necessarily form highly structured bilayers that would occur for simple amphiphiles, but rather a layer with more disorganized structure. We would expect that the most polar components would reside in the brine, forming a type of complex bilayer structure with a hydrophobic interior. The concept of line tension remains valid in general and it is probably the most essential parameter that determines the coalescence efficiency.

External forcing is needed to thin the interstitial oil film before coalescence can occur. The external force can be gravity or electric forces, or the inertia of colliding droplets. The draining process imposes hydrodynamic stress on the surfactant films, and this could promote film breaking provided that the stress is large enough to overcome the line tension. If the hydrodynamic stresses are not sufficient, then thermally induced stochastic fluctuations of the molecules may indeed serve to open up pores in the bilayer. A stable, dense packed emulsion in a bottle test is a good example of a case where hydrodynamic stresses had no effect on the coalescence of the remaining droplets. The thermally generated pores in the bilayer are either stable and close up, or they are unstable and will expand, leading to coalescence. This "tipping point" is given by a maximum energy in the bilayer, as we shall see in the next section. Local molecular configurations or "defects" in the bilayer may be an additional effect that can aid the purely stochastic and thermally generated pore formation process [144].

Demulsifiers can be added to promote emulsion breaking, and if they interact inside the bilayer, they may lead to morphology changes and result in structural heterogeneities in the mixture between surfactant and demulsifier. The line tension may now vary along the bilayer, with weaker regions being more prone to pore formation. DPD and molecular simulation are ideal tools for studying these processes in detail, and the addition of electric fields and ions opens up for in-depth studies of electrocoalescence.

5.1.2. *The DPD method in a nutshell*

DPD stands for Dissipative Particle Dynamics, a computational approach that belongs to the group of molecular simulation methods. The model molecules in DPD represent coarse grained approximations where groups of atoms are represented by "beads" with a certain mass, extension, and interaction force to other beads [145]. The main reason for choosing a coarse-grained approach is to speed up the computations and increase domain sizes beyond what is feasible with pure, fully resolved molecular simulations. This approximation comes at the cost of having to evaluate the interaction forces between the beads. These forces can be obtained in a rigorous bottom-up fashion by averaging over the resolved potentials arising from the detailed molecular structure [146] or one can choose a top-down approach by simply tuning the magnitude of the potentials to match the overall behavior of the specific system at hand. Water molecules are usually represented by single beads, complex fractions in oil by larger DPD molecules, and solvent oil may be represented by single beads again.

The coarse grained force between two beads of different type is repulsive due to a domination of the short range repulsive part of the single-atom interaction potentials. This force is energy conservative, and it is modelled by a linearly decreasing function with increasing bead distance up to a cutoff radius beyond which the force is set to zero. The linear part of the force can be expressed by a quadratic potential $\omega\,(r_{ij})$ in the bead distance r_{ij}:

$$U(r_{ij}) = a_{ij}\omega(r_{ij}) \tag{7}$$

where the matrix a_{ij} contains the adjustable set of interaction parameters between bead type i and j, and the normalized potential ω is usually taken to be the same for all conservative interactions.

To keep the beads in a molecule bound to each other, one uses a simple spring force between any two adjacent beads. This allows for long polymer chains and hydrocarbon side chains in larger molecules. Large assemblies of beads with fixed relative position to each other may represent large molecular entities such as carbon rings in asphaltenes, and multi-ring graphene type structures [147]. Such objects require more complex DPD algorithms to treat solid-body rotation. This is usually handled mathematically with quaternions (a complex number with one real part and three imaginary parts), an approach that is also used in computer games.

The molecules are set in motion by a stochastic driving force whose magnitude depends on the chosen kinetic temperature T_{kin} of the system in thermodynamic equilibrium. The corresponding energy input is balanced by a dissipative, frictional force opposing the motion of the beads. The balance between the driving and the dissipation brings the system to a thermodynamic equilibrium with time-invariant kinetic energy (or T_{kin}), and with equipartition of energy among the degrees of freedom (rotational and translational degrees). One can introduce external forces such as gravity and electric fields, and forces that describe interactions with solid surfaces so that adsorption processes can be incorporated. Solid surfaces can also be modelled by an assembly of beads.

It is relatively straightforward to incorporate different fluids in DPD by associating to them specific bead types. Immiscibility is provided by having stronger repulsion forces between unlike bead species than between like species. This provides spontaneous phase separation into oil and water domains, with the possibility of forming emulsion droplets. Stable emulsion systems with surfactants can then be studied, and the surfactant can be any molecular structure with hydrophilic and lipophilic ends. The simplest surfactant would consist of only two beads bound together by the spring force, where one bead is oil-loving and the other water-loving.

A proper set of surfactant-fluid interaction parameters results in a minimization of the total interaction energy (or mixing energy) when the surfactant resides on the interface between the fluids. The solubility of any surfactant can be controlled by the interaction parameters between the given fluid and the various surfactant beads. Any DPD molecule, including surfactant, is subject to thermal diffusion or Brownian motion in the solvent. A reduction of interfacial tension over time will then result by a net diffusion flux of surfactant to the interface, when one starts from a homogeneously mixed initial condition, out of equilibrium. The equilibrium state is further satisfying Langmuir type isotherms with a certain excess interfacial concentration larger than the bulk concentration.

The drawback with molecular simulations, also of the DPD type, is that only very small scales, up to the order of 0.1 μm along the edges of a simulation cube can be studied with a reasonable number of molecules (up to a million or so can be treated with normal workstations and parallel processing). These numbers depend on the level of coarse-graining in DPD. It is then only realistic to study micrometer-sized emulsions with only a few droplets in the cube. An alternative approach that is fruitful for pure coalescence studies is to "zoom up" on the interfaces such that one can treat them as flat with no significant curvature in the simulation domain. One can then study the molecular dynamics in great detail during the reconnection process between the two interfaces [148].

5.2. Electroporation theory as a "gedankenmodell" for electrocoalescence

DPD is a direct simulation method to study the fundamentals of coalescence, also with electric fields. Electroporation theory is a separate framework that can be used to generate coalescence rate models for an emulsion. DPD and experiments can then be used to develop constrained electroporation models for specific emulsion systems with surfactant and demulsifier.

Electroporation in phospholipid bilayers has been studied extensively in cell biological contexts, with poration of cell and vesicle membranes [142,143]. It is intriguing that electroporation theory would also describe the simplest emulsion system with brine droplets in oil, covered with amphiphilic, oil soluble surfactant. When the oil film is completely drained, the two surfactant layers form a bilayer membrane, and electroporation theory is therefore a natural starting point for the development of a phenomenological model for electrocoalescence in oil/water emulsions. This is an exciting case of interdisciplinary crossroads that needs more attention.

With some degree of charge separation in the brine, the droplets become polarized and there will be a net charge difference over the bilayer between two droplets. If the bilayer is impermeable for ion transport (non-conducting), the two layers of opposite charge correspond to an electric capacitor that can store electric energy. If a pore is initiated by thermal fluctuations, a part of this energy is removed locally. A lower energy configuration is preferable, and increasing pore size may reduce the total energy of the bilayer further so that the pore will expand indefinitely. This happens when the seeded pore radius is above a critical value. Electroporation theory shows that if the electric potential difference over the bilayer is increased, the critical pore size is reduced, so that the formation probability of unstable, expanding pores is higher. The ion concentration in the electrolyte and the applied field strength are the central variables that control the potential difference over the bilayer.

The energy required to generate a pore of radius r_p is[149],

$$E_p(r_p) = 2\pi\gamma_l r_p - \pi\gamma r_p^2 + E_i - \frac{\pi}{2}C_p\, V^2 r_p^2 \tag{8}$$

The term $2\pi\gamma r_p$ is the energy required to overcome the cohesive energy in opening the pore, and γ_L is the line tension. The term $-\pi\gamma r_p^2$ is the interfacial energy lost by replacing the surface with a hole, and γ is the interfacial tension. The term E_i can be added to represent the molecular interaction over the pore opening between the molecules that line the interior of the opening, and a possible surfactant bending energy associated to the interior of the pore. The crucial term in electroporation is $-\pi C_p\, V^2\, r_p^2$, the electric energy lost by replacing a section of the "membrane capacitor" with a hole, and the electric potential difference across the bilayer is V. The capacitance in question is

$$C_p = \frac{1}{h}\,(\epsilon_w - \epsilon_{bm})\varepsilon_0 \tag{9}$$

This is the difference in capacitance between the pore and the intact bilayer membrane, and h is the bilayer thickness or a few nanometers, and ϵ_w and ϵ_{bm} are the dielectric constants of water and bilayer membrane, and ε_0 is the permittivity of vacuum. C_p is of the order of 0.1 F per square meter. The capacitance per unit area of bilayer is $C_p = \frac{1}{h}\,\epsilon_{bm}\varepsilon_0$.

If the interaction term E_i in the pore can be neglected, it can be shown that the pore energy $E_p(r_p)$ has a global maximum value E_m of:

$$E_p(r_c) = E_m = \frac{\pi\gamma_L^2}{\gamma + \frac{C_p V^2}{2}} \tag{10}$$

at the critical pore radius

$$r_c = \frac{\gamma_L}{\gamma + \frac{C_p V^2}{2}} \tag{11}$$

If the seeded pore radius is above r_c, the pore is unstable and expands since the energy is reduced further for larger radii. If the seeded pore has a radius below the critical one, it closes up, also with an associated energy reduction. Characteristic values of the critical pore size r_c is in the

range 0.1–1 nm [149], with lower values for higher V. This formulation and what follows is of course valid also when the electric field is zero, and the ratio between line and interfacial tensions becomes the essential parameter.

First, it is clear that the electric energy has to be comparable or larger than the interfacial tension for the electric field to have any effect. It is noted that V increases with increasing charge density in the electrolyte near the bilayer, and increasing applied field strength (applied background potential). It is also clear that lowered line tension lowers the energy threshold E_m and the critical pore radius r_c, so that the coalescence probability increases. In essence, electroporation theory predicts larger coalescence rates by lowering the line tension, and by increasing the membrane potential difference V. The change of interfacial tension would modulate value of the critical pore size, with larger interfacial tension corresponding to smaller critical pore size.

Both the line tension and the surface tension will be modified by the addition of demulsifier. In absence of experimental data on line tension for crude oil systems, we can only speculate on this variations of this parameter. We may expect that the line tension decreases when a demulsifier is mixed into the surfactant layer, so that less energy will be required to open a pore. A reduction in line tension is also possible through a reduction of surfactant/demulsifier surface density locally through aggregation, or more globally by desorption of surfactant by the demulsifier. If the surface coverage or area fraction of demulsifier is very small compared to that of the surfactant, we may expect that significant changes to the interface can occur only locally through local clustering or aggregation of demulsifier. It is well-known through experiment that the interfacial tension may be altered by adding demulsifier. Desorption of surfactant increases the interfacial tension, while a coexisting surfactant/demulsifier layer may reduce the interfacial tension (IFT), depending on demulsifier properties. Pradilla et al. found that the interfacial tension was reduced when a model demulsifier was added to an asphaltene system [150]. If the demulsifier replaces some of the surfactant at the interface, the IFT may decrease if the demulsifier is more surface active, or the IFT may decrease if both the surfactant and the demulsifier coexist at a higher surface density.

It is noted that the given electroporation model does not incorporate interfacial curvature energy at larger scales. The theory would then best represent flat contact areas between droplets before the electric field is turned on, and this may be realized for dense-packed emulsions.

Once a pore opens, free ions in the electrolyte will start moving through the pore opening and cancel the charge difference. Despite of this, coalescence will proceed unhindered as long as the pore is large enough to be unstable and expanding. One could also imagine that bilayers of more complex molecules could be semi-permeable for ions (slightly conducting), and this would reduce the charge difference over time prior to pore formation, and the likelihood of a coalescence event would diminish with time after the droplets are brought into contact.

5.2.1. The emulsion coalescence rate derived from electroporation theory

A probability distribution of the waiting time from two droplets are brought together and to the formation of unstable pores can be derived from electroporation theory. The complete waiting time would incorporate the draining of the liquid film between the drops, but this is covered by hydrodynamic film draining theory. The average formation frequency of unstable pores (events/s) in an emulsion can be written [142]:

$$f = f_0 V_m e^{-\frac{E_m}{kT}} \tag{12}$$

where f_0 is a characteristic frequency per volume, $V_m = hA$ is the total bilayer volume in the emulsion with A the total contact area between droplets. This form already captures the effect of increasing pore formation frequency with increasing temperature.

The local charge density over the membrane is fluctuating due to thermal motion of the ions. The critical pore radius and energy are then stochastic quantities in terms of the fluctuating potential difference $\widehat{V} = V_0 + \delta V$. The variance of δV is determined by the fluctuations in ion density, and the average value V_0 is determined largely by the average ion density near the interface, and to some degree the external potential. The magnitude of the average ion density near the interface increases with applied field strength (through charge separation). One may assume that δV and V_0 are both proportional to the applied field strength to first approximation. Ion mobility, the drift timescale in response to temporal changes in the applied filed, and the direct influence from temperature of the ion density fluctuations can be taken into account for the next level of approximation.

We can now adopt the stochastic varieties:

$$E_m = \frac{\pi\gamma_L^2}{\gamma + \frac{C_p \widehat{V}^2}{2}} \tag{13}$$

and

$$r_c = \frac{\gamma_L}{\gamma + \frac{C_p \widehat{V}^2}{2}} \tag{14}$$

The maximum energy of a pore now has a probability density $p(E_m)$, due to the fluctuations in $\widehat{V}$.The average pore formation frequency is then

$$f = f_0 V_m \int_0^\infty e^{-\frac{E_m}{kT}} p(E_m) dE_m \tag{15}$$

This constitutes a model for the expectation value of the coalescence frequency in the emulsion, with the effect of demulsifier and electric fields. The probability distribution for a given number of events to occur in a certain time interval is likely to be Poisson distributed with a mean number of events per unit time equal to f. This would constitute the waiting time distribution.

The integral for f can easily be evaluated numerically once $p(E_m)$ is determined. To make the predictions from this integral more transparent here, we assume small fluctuations $|\delta V| \ll V_0$ that will occur for sufficiently low temperatures. The probability distribution $p(E_m)$ now tends to a Dirac delta function (a spike at a certain value $E_m(V_0)$ and zero elsewhere), and the integral reduces to

$$f = f_0 V_m exp\left\{ -\frac{1}{kT} \frac{\pi\gamma_L^2}{\gamma + \frac{C_p V_0^2}{2}} \right\} \tag{16}$$

The coalescence frequency increases with lowered line tension, higher electric potential and increased temperature, as expected. The maximum value for vanishing line tension is given by $f_0 V_m$, and $f_0$can be regarded as a tuning parameter that can be determined by experiment. The impact of the temperature dependent width of the distribution $p\left(\widehat{V}\right)$ (likely a truncated Gaussian) can be evaluated by numerical integration or by approximate analytic solutions. This will however only provide higher order corrections to the given formula.

The exponential variation of the coalescence frequency in any of the variables suggests that one may define regimes where coalescence is highly probable or highly improbable. The transition between these regimes constitutes a threshold value for coalescence to occur in terms of the given variable. The threshold can be found by setting the bracket in the exponential above to unity. The threshold value V_T for the potential difference V_0 is

$$V_T = \sqrt{\frac{2}{C_p}\left(\frac{\pi\gamma_L^2}{kT} - \gamma\right)} \tag{17}$$

It is noted that coalescence can occur with no electric field, provided that the line tension is sufficiently low so that $V_T = 0$.

Fig. 9 shows the exponential variation of the pore formation delay defined by $T = \frac{1}{f} + T_s$, to represent data from specific DPD simulations [148]. The threshold potential difference is here about 0.5 Volt. This is in fact comparable to transmembrane voltages reported for electroporation of phospholipid cell membranes [142,151,152]. The pore formation delay measured after the DC field was turned on in the DPD simulations had an additional contribution from the initial charge separation of duration T_s. For the stronger fields, the waiting time converges to T_s as shown. The waiting time can span from extremely small values in comparison to the hydrodynamic film draining time (strong fields) to extremely large values with essentially no coalescence (weak fields). The model predicts increased coalescence rate with demulsifier as long as the line tension or cohesive energy is reduced by the addition of demulsifier. It is seen from Eq. (16) that the coalescence frequency increases for reduced line tension.

5.2.2. Experimental testing

The line tension and interfacial tension of a specific combination of demulsifier and surfactant must be measured in order to generate predictions of the coalescence rate, according to the formulae above. To test the theory, one would also need estimates of the coalescence frequency or waiting time. We suggest that poration events could be detected by measuring the current through a larger scale bilayer membrane, or by monitoring individual coalescence events in a dense packed emulsion after a DC field is turned on. One can then correlate the findings to the predictions from electroporation theory.

The line tension and interfacial tension would be unique "global" quantities on the interface for well-defined surfactants. This is not necessarily so when demulsifier is added. Morphology changes and heterogeneities may develop with associated fluctuations of both the line- and interfacial tension along the interface. The molecular organization in interfaces are difficult to measure, and advanced experimental studies could be developed. Neutron scattering techniques that could work for liquid-liquid interfaces [153], AFM (atomic force microscopy) works for adsorbed surfactant layers on dry surfaces [154] and for free standing polymer membranes [155], while one can use small angle X-ray scattering techniques [156] to study surfactant-demulsifier interactions. The "mainstream" experimental technique for line tension is to measure the variations of the contact angle with the volume of the drop. The line tension slightly modifies the apparent contact angle and this effect becomes lower and lower when the drop volume increases. However, the experiments are very difficult to do because the effect is very small [157].

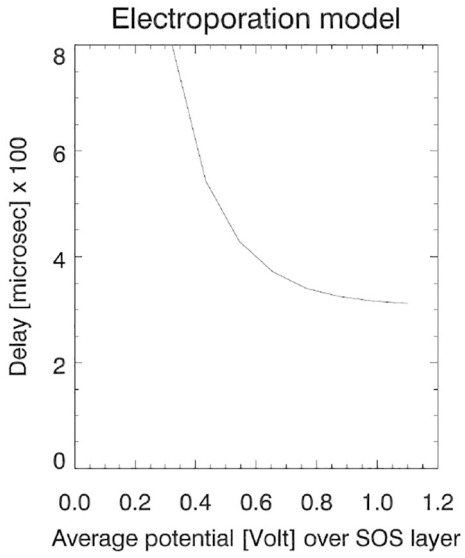

Fig. 9. Electroporation theory predicts a rapid variation of the pore formation delay 1/f as function of $\mathbf{V_0}$. This example represents a best fit to data from DPD simulations[148]. The surfactant-oil-surfactant (SOS) layer in the DPD simulations is a very thin oil layer coated with surfactant towards the two adjacent water domains. The energy considerations for the SOS layer is similar to that of the bilayer, so that electroporation theory can be used. From Skartlien et al. [148] - Published by The Royal Society of Chemistry.

Additional electrostatic modelling would be needed to estimate the characteristic potential difference over the bilayers in an emulsion. For AC fields, one would also need to consider ion mobility and the timescale of charge separation against the AC frequency. Higher frequency would imply less charge separation and less efficient coalescence, if the AC period is much smaller than the mobility timescale of the ions (the ions would then move less for higher frequency).

5.2.3. Insights from electrostatic DPD simulations

An electrostatic DPD code can incorporate realistic combinations of both indigenous surfactant (e.g., asphaltenes) and more detailed demulsifier structures. Electrostatic DPD have been implemented to study polyelectrolytes [158], acid/base reactions including proton transfer [159] and recently by our group with partitioning of acids over oil/water interfaces [160]. For water-in-oil coalescence studies, we incorporated ions in the water, an external electric field, and varying surfactant density and chemical structures [148].

For electrolytes such as brine, one can assume electrostatic conditions and solve only the Poisson equation for the electric potential, given the charge distribution in the electrolyte:

$$\nabla \cdot (\varepsilon \nabla \varphi) = -e n_q \tag{18}$$

where n_q is the net charge number density, φ is the electric potential, e is the elementary charge, and the electric field is $\boldsymbol{E} = -\nabla \varphi$. The electric force on a DPD bead is $\boldsymbol{F} = q\,\boldsymbol{E}$, with q being the total charge on the DPD bead. Thus, one solves the Poisson equation for every timestep, and then updates the bead positions after evaluating the force on every bead. The new bead positions alter the charge distribution in space, and the Poisson equation is solved again in the next timestep.

One resorts to a spatial smoothing of the charges to provide numerical stability, rather than using the point charges directly [161]. The Poisson equation can be solved by iteration (for every timestep), similar to the iterative solution of a diffusion equation. The convergence can be slow, and it is then an advantage to start from the potential obtained at the previous timestep, as this will be close to the solution for the next timestep. This approach will for example result in the classical equilibrium configuration of charged double layers as described by Poisson-Boltzmann theory.

Fig. 10 shows an example of our DPD simulations, representing the flat contact area between brine droplets in dense-packed emulsions [148]. These simulations are meant to represent droplets that are already in close contact before a DC field is turned on. We also assumed a remaining interstitial oil film between the surfactant layers rather than a pure bilayer. The surfactant-oil-surfactant structure was named the SOS layer for short. The energy considerations for the SOS layer is similar to that of the bilayer with effective line tension, capacitance and interfacial tension, so that electroporation theory could be used to interpret the simulation data.

The full duration of the simulations was about one microsecond. The external electric field strength and the cohesive energy between the surfactant molecules were varied. The electric field was applied over the domain perpendicular to the SOS layer, and had three values E = 0.0,0.5,1.0 normalized to 18 kV/cm. The maximum value of 18 kV/cm is moderately larger than for a typical electrocoalescence case with a field strength of a few kV/cm. The potential difference over the thin SOS layer of a few nanometers is only of the order of 0.1–1.0 Volt at the charge densities used. The direct contribution to the potential difference from the external field is only marginal. The major contribution comes from the local charge difference over the SOS layer.

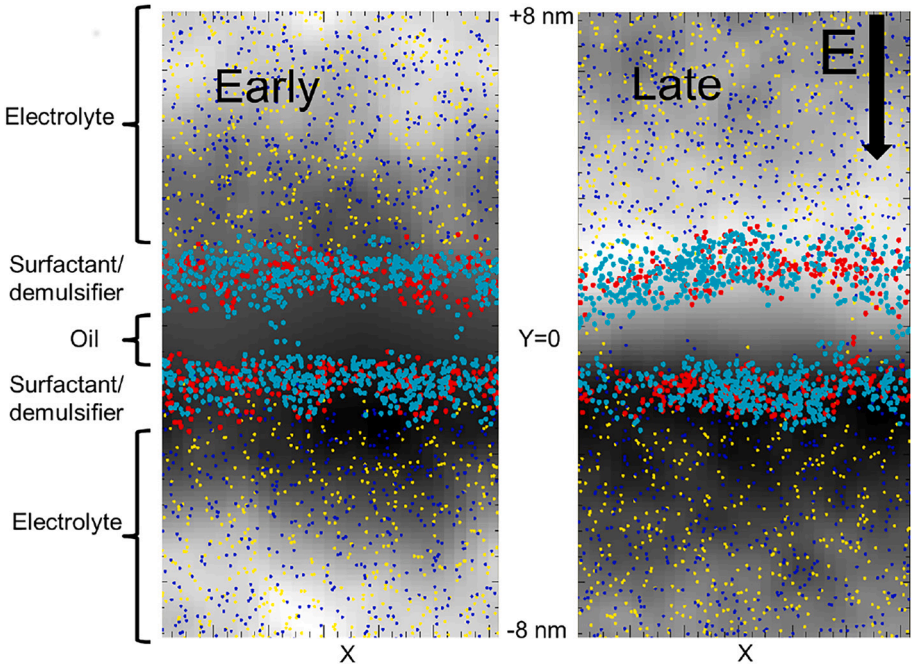

Fig. 10. An overview of the simulation domain at early (close to the initial condition) and at late times after charge separation has had time to relax. The electric potential deviation from the time averaged potential is shown by the grey scale. At late times, the potential difference over the surfactant and oil layers (SOS layer) is elevated, and poration occurred spontaneously. The *E*-forces on the ions pinches the SOS-layer centered at y = 0. Yellow symbols show positive ions (Na), while blue symbols show negative ions (Cl). The surfactant is marked with red symbols, and the demulsifier with turquoise symbols. Both species are located at the oil/water interface. From Skartlien et al. [148] - Published by The Royal Society of Chemistry.

The number of water beads was 9000, the number of oil beads was 1200, the number of surfactant and demulsifier beads was 1800, and the number of ions in the water was 1800. The bulk ion concentration was about 25% by volume and charge neutrality was imposed. The elevated ion concentration relative to brine was chosen to have a sufficient poration probability in the small domain, and over the duration of the simulation. Nearly full coverage on the interface of surfactant and demulsifier was implemented to achieve significant stability against coalescence without the electric field.

The opposite charges over the SOS layer provided a perpendicular, compressive electric forcing on the SOS layer. Thermal ionic density fluctuations (seen in Fig. 10 via the fluctuations in the potential as a varying grey-scale) resulted in a stochastic component to the forcing with excess magnitude in local areas that could lead to unstable expanding pores there. Current flowed through the expanding pore in the SOS layer with a gradual elimination of the charge difference between the two electrolytic (brine) domains (Fig. 11).

The demulsifier was modelled as an amphiphile with varying interaction with the surfactant, with strong repulsion between the demulsifier and the surfactant (incompatible demulsifier with respect to the surfactant) and then with attraction between the demulsifier and the surfactant. Attraction means simply that the two compounds are mutually soluble, and repulsion means that they are less soluble into each other. Furthermore, the demulsifier and the surfactant were chosen to have similar surfactant behavior with respect to the oil and water. We adopted the corresponding a_{ij} values (defined in Eq. (7)) from Li et al.

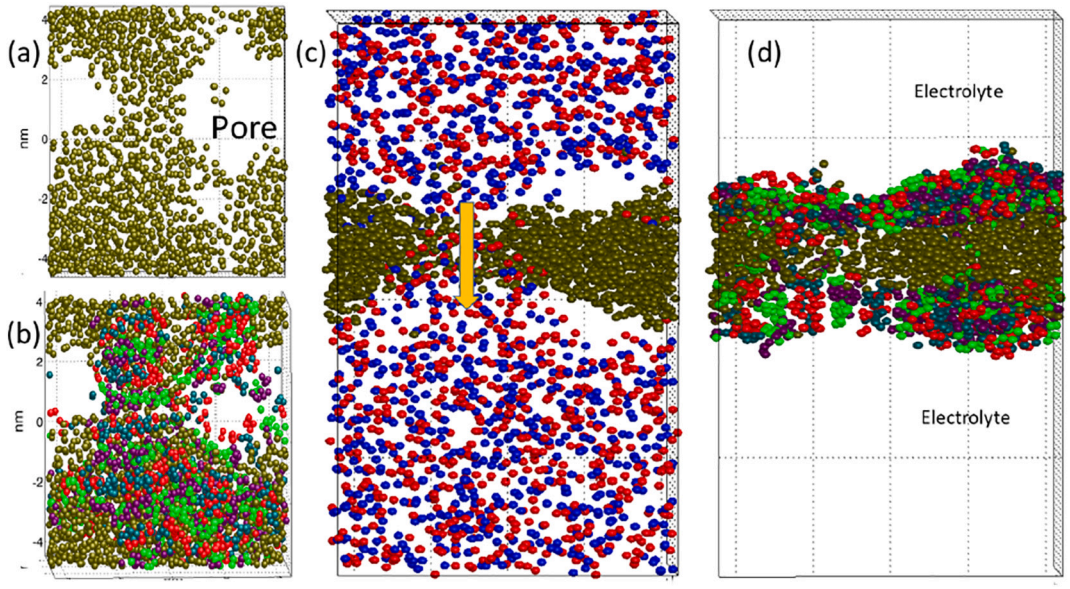

Fig. 11. Panel (a) shows a developed pore through the thin oil layer, and Panel (b) shows the surfactant and demulsifier as well. The surfactant is shown with red (polar beads) and green (chain beads) and the demulsifier is shown with turquoise (polar beads) and violet (chain beads). Panel (c): A side view with positive (red) and negative (blue) ions in the brine. Panel (d): The same side view with oil and surfactant/demulsifier mixture showing. The horizontal extent of the domain is 8.1 × 8.1 nm, and the vertical extent is 15.9 nm. From Skartlien et al. [148] - Published by The Royal Society of Chemistry.

[162] for sodium dodecylbenzene sulfonate (SDBS), an interfacially active molecule that is more soluble in oil than in water (due to its long hydrocarbon chain).

In DPD, all forces are indeed repulsive and all interaction parameters $a_{i\ j}$are positive, as described earlier. However, an effective attraction between two beads will result when the repulsive force between them is smaller than the repulsive force to other, surrounding beads. An effective repulsion will occur when the DPD force between two beads is greater than the repulsion to surrounding beads. The effect of the interactions between the demulsifier and the surfactant were adjusted via the forces between the polar parts ("head beads", H) and the hydrophobic parts ("tail beads", T). The surfactant D had the bead structure H-H-T-T, and the demulsifier h-h-t-t (uppercase and lowercase distinguishing the beads types). The forces between H and h and between T and t were varied to produce repulsion (high $a_{H,\ h}$ and $a_{T,\ t}$ parameters) and attraction (low $a_{H,\ h}$ and $a_{T,\ t}$ parameters). These particular interaction parameters were considered to be free variables to obtain clear attraction and repulsion (solubility) effects between the demulsifier and the surfactant. Their magnitudes were however constrained to be similar to the "surfactant interaction parameters" between the demulsifier or the surfactant and oil/water.

Repulsion lead to islands of demulsifier and surfactant domains in the interface and this allowed for lower interfacial concentration at the borders between the domains, reducing the local line tension there. Attraction between demulsifier and surfactant leads to aggregation of surfactant and demulsifier as shown in Fig. 11, leaving larger vacated areas of exposed oil film. The line tension is reduced considerably in these areas, leading to more efficient pore formation than in the first scenario. Aggregation may, in a real system, correspond to the interaction between demulsifier polar groups that are able to attract and interact strongly with the surfactant polar groups. This is expected for the typical petroleum demulsifier, with long polymer segments that can attach to a larger number of surface-active molecules. Another interesting finding was that incompatible demulsifier resulted in pores in the oil film that could be partially filled with a surfactant and demulsifier mix. If not leading to coalescence, these filled pores could be electrically conducting and eventually neutralize the electric forcing of the bilayer.

The most important outcome of these electrostatic DPD simulations was the realization that morphological change in the surfactant layer induced by the demulsifier, determined to a large degree where pores formed. Electroporation theory can indeed be used to generate a coalescence model, but the DPD results suggest that one would need to consider interfacial and line tensions as local quantities that vary across the interface. One would then also need to consider the statistics of these fluctuations in a more generalized version of electroporation theory. Another important outcome was that ion density fluctuations is an essential ingredient at these small length scales. The associated fluctuations in the electric potential over the bilayer should be incorporated into the electroporation theory as shown, when it is used for electrocoalescence.

6. NMR to monitor emulsions destabilization in electric fields

6.1. Interest

Central processes in emulsions that characterize the state of the emulsions are sedimentation (creaming), flocculation and coalescence. Obviously, we want to observe these parameters as a function of time for emulsified water droplets under experimental conditions manageable for NMR. We start with a brief definition of these processes. The sedimentation process is gravity driven and follow Stokes law for an ideal case. For dilute systems without any droplet interactions, the sedimentation velocity is:

$$v = \frac{2}{9}\frac{(\rho_d - \rho_m)}{\mu_m} g R_d^2 \tag{19}$$

Some parameters are defined in sections 3.1 and 2.4 and are recalled here for sake of clarity: v: sedimentation (or creaming) velocity (or sedimentation rate), ρ_d and ρ_f are the densities of the droplet and the dispersing medium respectively, μ_m is the dynamic viscosity of the dispersing medium, g is the gravitational field strength, and R_d is the droplet radius.

Obviously significant parameters are the viscosity of the continuous phase, density difference between dispersed and continuous phase, gravity and the droplet size. In order to estimate the sedimentation rate, we need information about droplet sizes and changes in these. The sedimentation process is an important process parameter. It accounts for a redistribution of water droplets and the formation of local droplet concentration gradients that are important for the stability / destabilization of the emulsions. For oil-in-water emulsions the corresponding parameter is creaming where the flow pattern of droplets is upwards mainly due to density differences. The sedimentation / creaming process can give rise to process phenomena where a dense packed layer (DPL) can occur in a separator [163,164]. In the DPL the concentration of droplets can be as high as 70% which corresponds to an efficient packing of droplets from geometrical consideration. It has been documented that the stability mechanisms of these droplets are quite different from lower concentrations. For the sedimentation process we must use NMR to determine the initial droplet sizes and the changes in water content along the axis of the gravity, i.e. the brine profile [165–167]. The sedimentation process is inevitably related to the coalescence process as droplets merge. We expect an increase in size and decrease in number. Then, the evolution of the brine profile will provide a measure of the sedimentation rate and indirectly the speed of coalescence.

NMR is a noninvasive tool for characterizing emulsions, and it does not require the system be transparent, as optical methods do. Furthermore, it characterizes the total measuring volume and not only the surface visible by optical means. In the following the NMR methods for monitoring the time dependency of the brine profile and measuring droplet size distribution will be discussed accompanied with examples of applications. During emulsion separation there is a sedimentation process going on, i.e. water droplets coalescing and moving towards the bottom to form a bulk water phase. This will lead to an extra convection phase term in the equation for the NMR signal [168], but as this paper is concerned with a NMR signal in real time and in magnitude mode, the convection term from the sedimentation does not affect the results of the NMR experiments as discussed in the following.

6.2. The determination of brine profiles

As the emulsion contains both crude oil and brine, and our LF-NMR (Low Field-Nuclear Magnetic Resonance) instrumentation do not allow a NMR signal that can be resolved in frequency, one of the dynamic parameters relaxation times T_1 or T_2 (respectively the longitudinal (or spin-lattice) and the transverse (or spin-spin) relaxation times) or Diffusion must be used to resolve the brine signal from the crude oil signal [169]. These relaxation times quantify the return of the magnetization to its equilibrium and depends on the molecular mobility. In Fig. 12 we have applied a pulse sequence where an initial loop of C1 echoes is applied to suppress the contribution from crude oil. The assumption is then that the T_2 relaxation time of the crude oil is significantly shorter than the T_2 of the brine. This is equivalent to saying that the viscosity of the crude oil must be significantly higher than the viscosity of the brine.

When imposing a magnetic field gradient during the acquisition at t_1 and t_2, we may get a 1-dimensional image of the brine signal after performing a Fourier transform of the acquired signal. Also, the brine content of the emulsion can be found by performing an exponential fit of the echo signals I_1 and I_2 at t_1 and t_2 respectively, yielding I_0. Then the 1-dimensional image can be rescaled to provide the actual brine content as a function of position in the sample, the brine profile.

In Fig. 13 the brine profiles of three different samples of the same

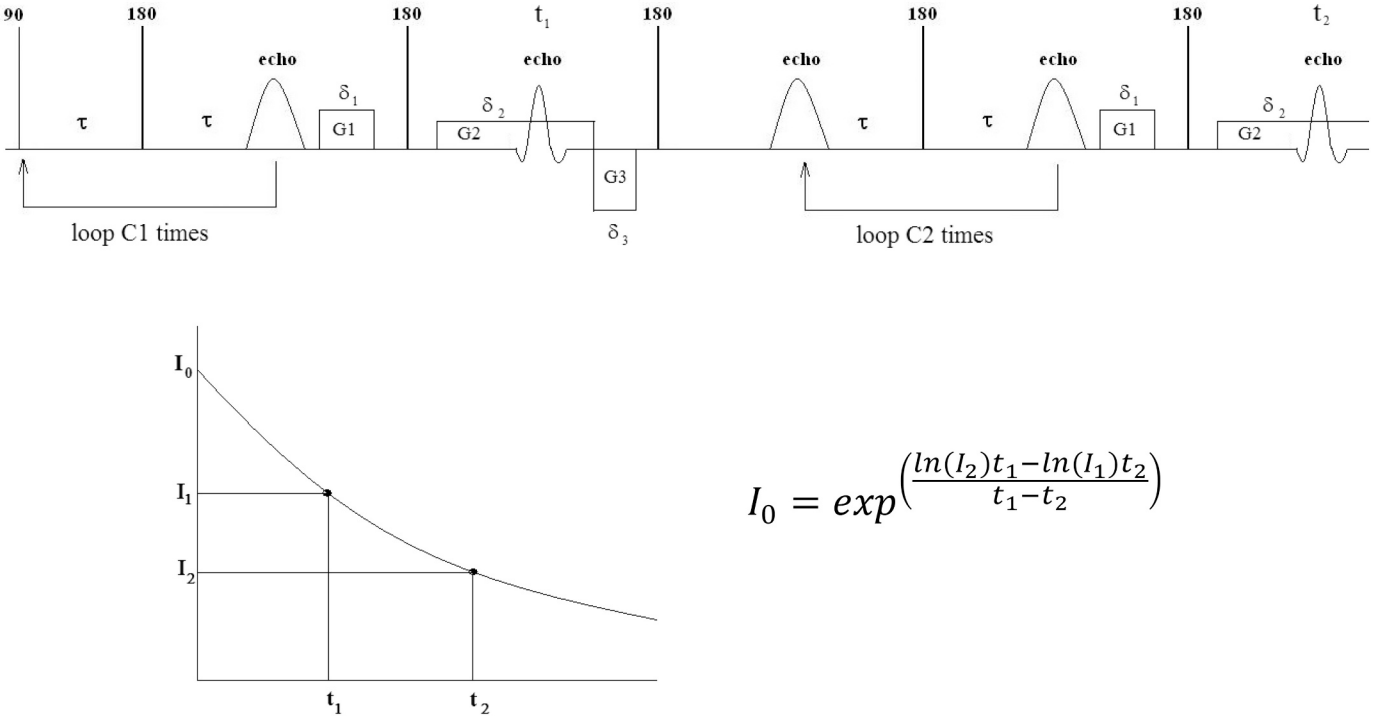

Fig. 12. The NMR pulse sequence for acquiring the brine profile (top) and the principle to obtain a quantitative water profile by extrapolation of the signal (bottom). 2τ is the inter echo spacing, G1, G2 and G3 are applied magnetic field gradients, 90 and 180 denote the RF -pulses, C1 and C2 denote the number of echoes run before acquiring the brine profile, and t_1 and t_2 are the timings for acquiring the brine profile. The equation to perform the quantification is also given. From Sørland [169].. Reprinted by permission from Springer.

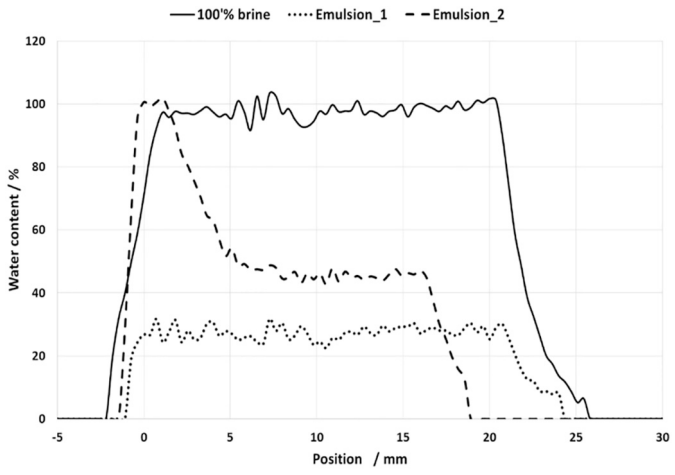

Fig. 13. Brine-profiles of pure brine, one stable (Emulsion_1) and one unstable emulsion (Emulsion_2). From Sørland [169]. Reprinted by permission from Springer.

length are shown. The pure brine results in a brine content of 100% along the sample while the stable emulsion, Emulsion_1, also shows a constant brine content of approximately 30%. Thus, the water cut of this emulsion is said to be 30%. For the unstable emulsion, Emulsion_2, we see that the brine droplets have coalesced and sedimented to form a bulk brine phase at the bottom of the sample, the a region of emulsion of ~45% water cut, while on the top 5 mm of the sample there is crude oil only.

6.3. The determination of droplet size distributions

As shown by Mitra et al. [170], the solution of the diffusion propagator in restricted geometries does not contain the surface relaxation term in the first order correction term to bulk diffusion coefficient at short observation times. When assuming piecewise smooth and plane surfaces and that only a small fraction of the particles is in contact with the restricting geometries, the restricted diffusion coefficient can be written as:

$$\frac{D(t)}{D_0} \approx 1 - \frac{4}{9\sqrt{\pi}}\sqrt{D_0 t}\,\frac{S}{V_d} + \varphi(\rho, r, t) \tag{20}$$

where $D(t)$ is the time dependent diffusion coefficient, D_0 is the unrestricted diffusion coefficient, in bulk fluid, and t is the observation time. The higher order terms in t, $\varphi(\rho,r,t)$ include the deviation due to finite surface relaxivity (defined in section 6.3.1) and curvature (r) of the surfaces. At the shortest observation times these terms can be neglected and then the deviation from bulk diffusion depends on the surface to volume ratio alone.

In a heterogeneous system as an emulsion a variation in droplet sizes must be assumed. However, Eq. (20) is valid for a heterogeneous system as long as the assumptions leading to are fulfilled for all droplet sizes. If ξ_i is the volume fraction of the pores (in the emulsion case, droplets) with surface to volume ratio $(S/V_d)_i$, Eq. (20) can be expressed as:

$$\sum_i \xi_i \frac{D_i}{D_0} \approx \sum_i \xi_i \left[1 - \frac{4}{9\sqrt{\pi}}\sqrt{D_0 t}\left(\frac{S}{V_d}\right)_i\right] = \left(1 - \frac{4}{9\sqrt{\pi}}\sqrt{D_0 t}\,\overline{\left(\frac{S}{V_d}\right)}\right) \tag{21}$$

Consequently, measurements of the early departure from bulk diffusion combined with a linear fit of the experimental data to the square root of time will result in a value for the average surface to volume ratio $\overline{\left(S/V_d\right)}$.

6.3.1. Transforming a T_2 distribution to a droplet size distribution

When assuming the water molecules to probe the restrictions of the

droplets in the fast diffusion limit, there is a simple relation [171] between T_2 values and the droplet sizes:

$$T_2 \approx \frac{V}{S\rho} \tag{22}$$

As this couples the surface to volume ratio to the surface relaxivity, ρ, it is not straight forward to assign the T_2 distribution to a (V/S) distribution. However, by assuming that Eq. (22) holds for any droplet size, with ξ_i being the volume fraction of droplets with surface to volume ratio $(S/V)_i$ and the corresponding relaxation time T_{2i}, we shall follow Uh and Watson [172] and write:

$$\sum_{i=1}^{n} \xi_i \frac{1}{T_{2i}} = \sum_{i=1}^{n} \xi_i \rho_i \left(\frac{S}{V_d}\right) \approx \rho \sum_{i=1}^{n} \xi_i \left(\frac{S}{V_d}\right)_I \approx \rho \overline{\left(\frac{S}{V_d}\right)} \tag{23}$$

Here the basic assumption is made that the surface relaxivity ρ is independent of droplet size. The left-hand side of Eq. (23) is then the harmonic mean $\overline{1/T_2}$ of the T_2-distribution weighted by the fraction ξ_i of nuclei with relaxation time T_{2i} and n is the number of subdivisions of droplet sizes. The left-hand side can be calculated from the T_2-distribution obtained from a CPMG measurement (Carr-Purcell-Meiboom-Gill sequence [173]) where the magnetization attenuation $M^{obs}(t)$ is converted to a T_2 distribution using an Inverse Laplace Transform (ILT) routine [174]. Then the surface relaxivity ρ can be calculated from Eq. (23) as the average value for the surface to volume ratio $\overline{\left(S/V_d\right)}$ is already found from the diffusion experiment. Then, the measured T_2-distribution is transformed into an absolute droplet size distribution (V/S) by means of the relationship inherent in Eq. (23).

The procedure for deriving absolute droplet size distributions can be summed up as follows:

1) The average surface to volume ratio $\overline{\left(S/V_d\right)}$ is found from fitting Eq. (21) to a set of experimentally determined apparent diffusion coefficients at short observation times.
2) The average (S/V) is then applied together with the average $(1/T_2)$ found from a CPMG experiment. From Eq. (23) Eq. (22) is then written as

$$\overline{\left(\frac{1}{T_2}\right)} \approx \rho \overline{\left(\frac{S}{V_d}\right)} \Rightarrow \rho = \overline{\left(\frac{1}{T_2}\right)} \times \overline{\left(\frac{S}{V_d}\right)}^{-1} \tag{24}$$

hence the relaxivity, ρ, is quantified and is assumed to be droplet size independent.

3) When assuming that the surface relaxitivity is independent of the droplet size the value of ρ can be applied in Eq. (22) resulting in a linear relation between T_2 and the volume to surface ratio which is a measure of the droplet size. By multiplying the T_2 distribution by the calculated surface relaxivity the distribution is transformed to a droplet size distribution in absolute length units.

6.3.2. *The slice selective PFG-NMR method for determining DSD*

As we are interested in the droplet size distribution of the residual emulsion in the presence of separated bulk brine at the bottom, an NMR method that distinguishes the contribution from different regions is necessary. This can be done by using shapes RF pulses and a slice gradient prior to the pulse sequences used to determine the droplet size distribution. Such an initial part is shown in Fig. 14.

The next section will show the interest of NMR in the study of demulsification in electric fields.

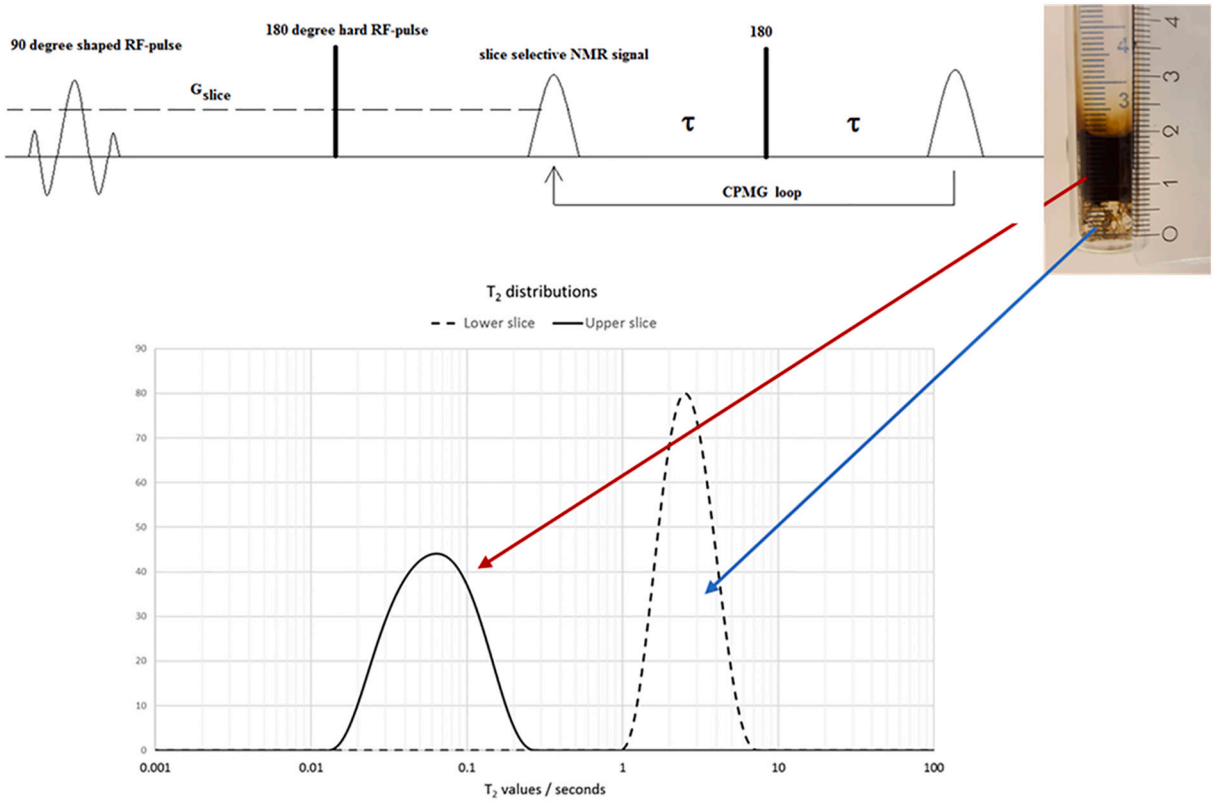

Fig. 14. Slice selection of the NMR signal to separate contribution from different phases followed by a CPMG experiment [173, 175]. Separate T2 distributions from crude oil (left) and brine (right) can then be produced.

6.4. Influence of chemicals on emulsions in electric fields studied by NMR

A convenient way to assess the influence of both chemicals (demulsifiers) and external electric fields is to use NMR. The parameters to be followed in order to map the stability of the emulsions is the change in droplet sizes and the immediate consequences for the sedimentation rates. Hjartnes et al. investigated heavy crude oils from The North Sea with 50 *v*/v % of water containing 3.5 wt% NaCl at an operationally relevant temperature of 65 °C[176]. Four different demulsifiers were added. They represented both commercially available ones and green candidates under development. The first assessment regarding the influence of the chemicals on the emulsified systems involves changes in the droplet populations. The corresponding distributions are displayed in Fig. 15 after a separation time of 2 h [176]. The droplets are centered around 10 to 15 μm with varying intensities. Two chemicals display a deviation from the first trend by a more pronounced width indicating larger droplets. The corresponding sedimentation times are higher and the deviation from theoretical values predicted by Stokes equation is about 100 times. The efficiency of the chemicals as measured from the appearance of free water is seen in Fig. 16. The coalescence efficiency of the investigated candidates varies both from samples and concentrations. Fig. 15 showed that some of the chemicals could keep in solution large droplets after the phase separation, which per se indicate different coalescence behavior. Fig. 17 reveals another aspect of the influence of the chemicals on the separation of the water from the emulsions. The figure is showing the residual water content as a function of the concentration of the demulsifier. It is tempting to say that the coalescence has two different time constant. The initial destabilization of the aqueous droplets is demanding small concentrations of demulsifier. The residual aqueous amount seems to need more demulsifier to meet the expectations. Perhaps the nature of the interfaces is different due to the higher amount of existing indigenous surfactants as a result of the coalescence process.

The next figures show the effect of an external field with and without chemicals on the emulsions described above. The idea of combining chemicals and external electric fields is to look for synergies between two different approaches. Fig. 18 reveals the combination of both chemistry and external voltage. An addition of 10 ppm of chemical 1 for 2 min shows very little deviation from applied electric field effect [55]. It takes longer time to observe the advantages with both AC treatment and chemicals. In the present case we prolonged the study to 2 h and found a clear acceleration of water separation for the lowest applied fields. Higher fields however, resulted in no significant changes.

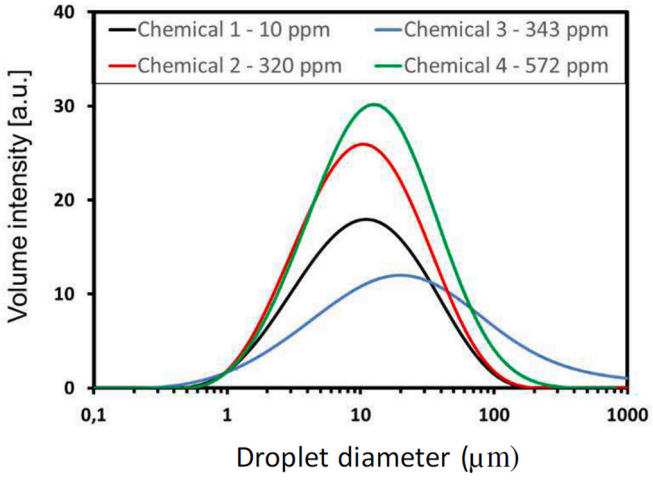

Fig. 15. Droplet size distribution of crude oil emulsions in presence of 4 different demulsifiers, measured after two hours separation. The demulsifiers were added right after emulsification. From Hjartnes et al. [176]. Reproduced with permission from American Chemical Society.

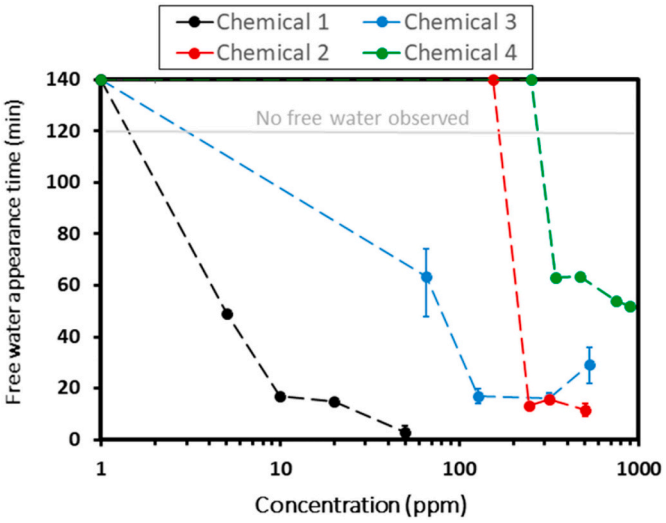

Fig. 16. Free water appearance time for crude oil emulsions in presence of 4 different demulsifiers as a function of demulsifier concentration. If no free water has appeared after 2 h separation, the time was indicated at the top of the curve. From Hjartnes et al. [176]. Reproduced with permission from American Chemical Society.

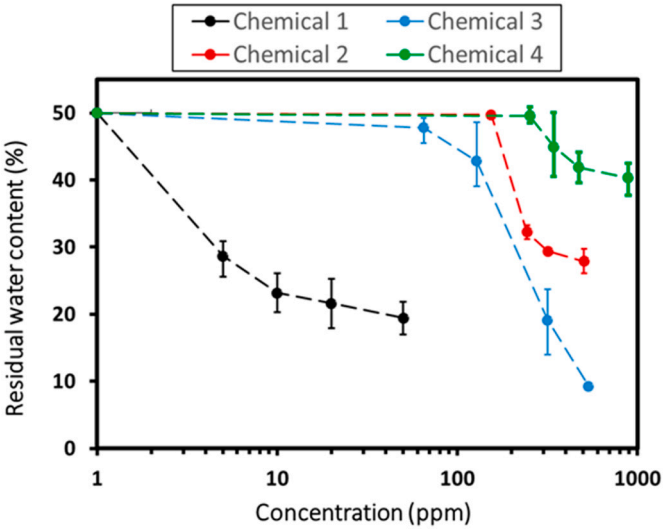

Fig. 17. Residual water content in the oil layer after two hours of separation for crude oil emulsions in presence of 4 different demulsifiers as a function of demulsifier concentration [176]. The residual content is defined as the water concentration measured at 75% of the sample height. From Hjartnes et al. [176]. Reproduced with permission from American Chemical Society.

Repeating the experiments for higher demulsifier concentrations reveals that there is limited effect of the chemicals above 100–150 ppm.

Combining chemicals and external electric fields is rather complicated. The number of parameters is large including concentration, observation time, level of the external field among others. Hence it is not surprising that the combination of the two operations can go in both directions, i.e. an external field might strengthen the ability of the chemical to breakdown the emulsified system, but in some cases the effect might as well be the opposite. Indeed, it is visible from Fig. 18.b that the chemical 2 initially retards the coalescence of droplets at 200 V/cm when it is present [55].

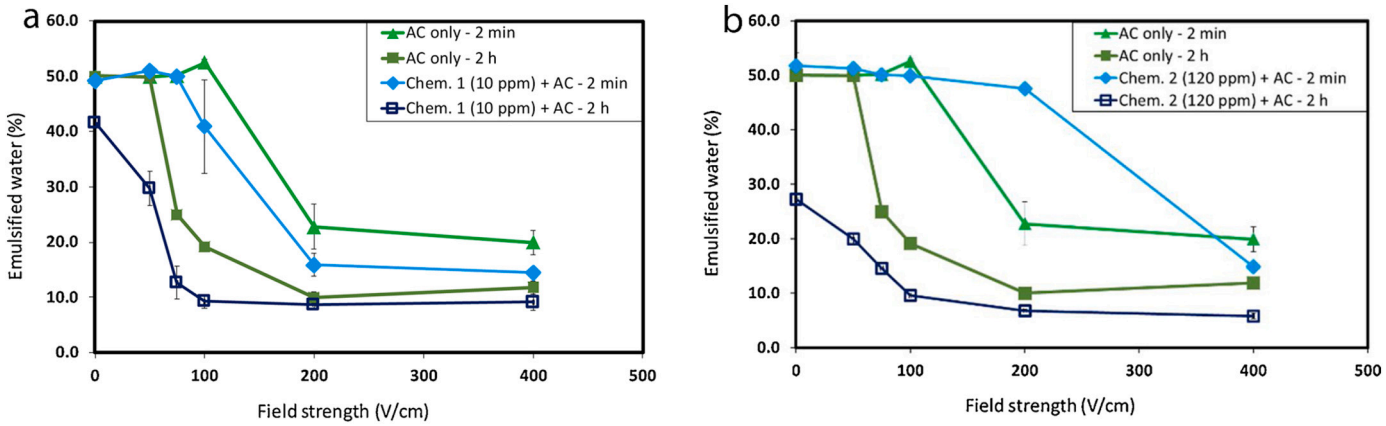

Fig. 18. Remaining emulsified water measured by NMR as a function of AC field strength for systems in presence or in absence of chemical demulsifiers. a): chemical 1, b): chemical 2. From Hjartnes et al. [55]. Reproduced with permission from Elsevier.

6.5. Other laboratory-scale batch techniques to assess the effect of electric fields on destabilization of emulsions

Apart from NMR that allows to follow up several parameters during emulsion destabilization, other techniques have also been developed. Two are presented in this section.

-The $E_{critical}$ (critical electric field) cell which is composed of a thin Teflon spacer placed between two brass plates. The Teflon spacer has a hole at its center. The two brass plates are connected to a power supply (see fig. 19.a). In a typical experiment, an emulsion sample is introduced in the Teflon spacer hole. Then a voltage (DC) is applied and increased linearly with time. The current is measured, and a sudden increase indicate the formation of a water bridge between the two plates indicating the destabilization of the emulsions. The electric field measured at the point of the increase is taken as a measure of the stability of the emulsion. This allows to compare various samples and study the effects of parameters such as the chemistry of the oil phase [53,177–180], the presence of demulsifiers [54], temperature etc. This technique is relatively easy to implement but it only provides one parameter summarizing the stability of emulsions under electric field.

Electrorheology [181,182] allows to study the effect of electric field on the rheological properties of water-in-oil emulsion. The technique is implemented with a rheometer fitted with a cylinder-cup geometry. The cylinder is linked to an electric power supply while the cup is grounded (see fig. 19b). In a typical experiment, the crude oil emulsion is introduced in the cylinder cup geometry and the viscosity is measured before, during and after the application of an electric field. The effect of various aspects of the field on the emulsion rheological's properties have been tested e.g. waveform, field strength and frequency.

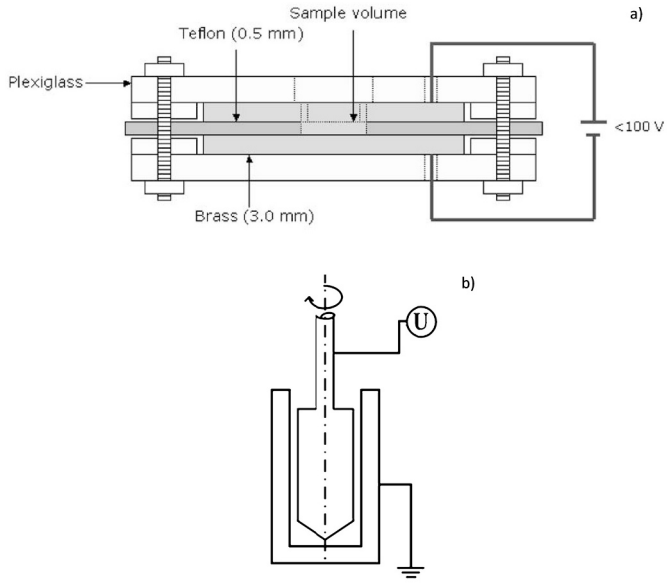

Fig. 19. Schematic drawing of a) the $E_{critical}$ (critical electric field) cell and b) the electrorheological cell. From Aske et al. [53] and Lesaint et al. [181]. Reproduced from permission from Elsevier.

7. Medium and large-scale destabilization of emulsions in electric fields

Although small scale experiments give positive indications on the effect of external electric fields on the separation of oil-continuous emulsions a final verification under realistic process conditions must be carried out. There has been an international interest to develop and commercialize the technology behind electrocoalescence. Many projects have passed through a development stage as prototypes and some to enter the market as commercially available instruments ready to install [183]. Examples are EPIC (Electro-Pulsed Inductive Coalescer), CEC (Compact Electrostatic Coalescer [184]), VIEC (Vessel Internal Electrostatic Coalescer [185–188]), IEC (Inline Electrostatic Coalescer [189]), LOWACC (Low Water Content Coalescer [190]). For large scale prototypes, the efficiency of the separation train must meet volume and time requirements. For normal crude oils the time constraint for the separation is about 4 min, while heavy crude oils can need much longer for the separation. The daily production rate can be as high as several 100,000 barrels per day. The quality criteria are such that an incoming well-fluid can contain up to 50% of water in oil while the outcoming processed fluid should meet export requirements on max 0.5% water in the crude oil. The separator mechanical internals to meet these process aspects are splash plates, pall boxes, and electrostatic units. In addition to the mechanical treatment it is also very common to use different kinds of demulsifiers to speed up the coalescence of water droplets. Especially the combination of chemicals and electrocoalescers seem to be promising.

Early versions of the commercial electrocoalescers had some shortcomings with regard to handling large amounts of emulsified water [185] and choice of electrode materials. Hence their operational mission in the separation train was more linked to a mission of desalter / dehydrator dealing with smaller amount of water. First out to solve these problems was VIEC (Vessel Internal Electrostatic Coalescer) originally produced by ABB (now manufactured by Sulzer). As an example of a large scale commercial coalescer, the VIEC device is schematically presented in Fig. 20.

As seen from the Fig. 20, the VIEC system is built up of elements

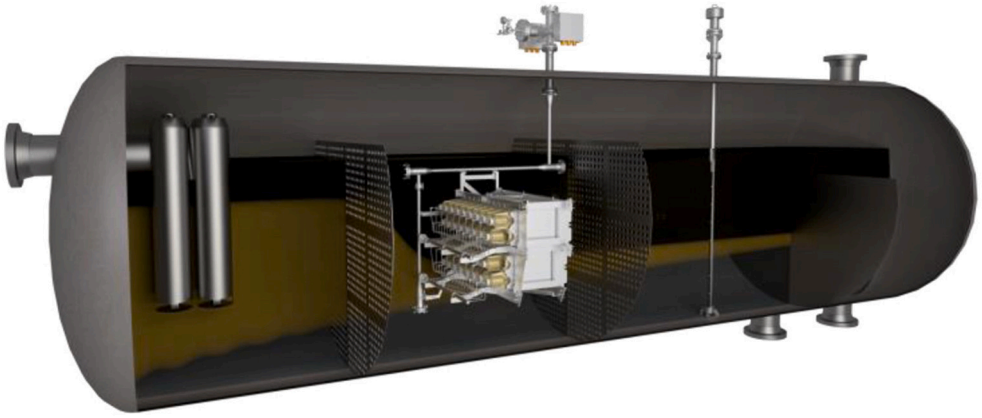

Fig. 20. A VIEC unit composed of multiple vertical electrode and internal transformer cast in an insulating material (yellowish element) installed in a gravity separator. From Amarzguioui and Jacobsen [185]. Reproduced with permission from Society of Petroleum Engineers.

consisting of single vertical electrodes cast in a specialized insulating material. The elements are installed inside a production separator in a modular manner in one or several walls of modules mounted in cassettes. The VIEC elements are energized by a low voltage feed penetrating the separator shell. The feed is transformed to high voltage in transformers molded inside each element. The elements are installed at a height exposed to an oil-continuous system. The figure further shows a typical VIEC unit inside the three-phase separator. The elements are supplied with a low-voltage high-frequency AC field by external frequency converter cards [185].

In order to prequalify for a world-wide use of VIEC at oil and gas producing fields large scale test were performed at full-scale multiphase test rigs with a wide range of crude oils and their emulsions [191]. Norsk Hydro (now Equinor) in Prosgrunn (Norway) extended the test program of the VIEC with regard to other material options.

The qualification of VIEC for field instalment started already in 2003 at Troll C in the North Sea [191]. The influence of the VIEC instalment became clear from the start. A more efficient separation became visible with the reduction of the emulsion band (dense packed layer, DPL). Other advantages were also imminent. A reduction of the demulsifier dosage from 10 to 2 ppm took place [191]. A consequence of this was seen on the interfacial control and better water quality. Both essential parameters in the separation process. The oil quality from the first stage separator continued to improve and the use of chemicals continued to decrease. After the success at the Troll C field the use of the VIEC escalated to China, Qatar [186], Brazil and Indonesia [192]. Obviously, the use of an efficient VIEC can make the whole train less complex by eliminating the second stage separator [190].

8. Conclusions

The purpose of the review article was to describe various phenomena happening at different scales during the destabilization of water-in-crude oil emulsions under electric fields (electrocoalescence). The important phenomena described according to the length scales are the following.

The oil-water interfacial properties i.e. interfacial tension, rheology and composition are important aspects controlling the coalescence and flocculation of water droplets. The interface is composed of asphaltenes and other crude oil components as well as chemical demulsifier. The application of an electric field induces fluid circulations across the drop interface. This phenomenon is called electrohydrodynamic (EHD) flows, which induces an increase in the adsorption rate of the surface-active compounds at the oil-water interface as shown by axisymmetric drop shape analysis taking into account Maxwell stresses.

At the drop scale, electric field induces deformation and motion of the droplets depending on the electrical and physical properties of the oil and aqueous phases. The strength of applied electric field is critical as an excessively strong electric field can lead to the drop breakup and reduction in average droplet size of the emulsion. The electric field-induced droplet motion by electrophoresis and dielectrophoresis may assist or inhibit coalescence.

The coalescence of two droplets occurs in three steps; first the approach of the droplets, then the drainage of the oil film between two droplets and finally the thin film breakup. Electric field favors attraction between droplets by inducing dipolar forces between adjacent droplets. The factors influencing the rate of drop-drop approach and film thinning as well as the conditions that aid film breakup and complete coalescence were detailed. Further, partial coalescence where the drop-drop or drop-interface coalescence maybe followed by generation of minute droplets was discussed. Dissipative Particle Dynamics molecular simulation (DPD) can help to understand the coalescence between droplets. This method simulates the last stage of coalescence by considering the pore formation in a surfactant laden oil film between two aqueous electrolyte layers in a DC field. DPD simulation results were found to compare well with electroporation theory.

Various techniques have been developed to study the effect of electric field on the emulsion resolution at the bench scale. Low Field-Nuclear Magnetic Resonance (LF-NMR) appears to be an attractive technique to follow-up and study crude oil-water separation. This non-invasive technique is not influenced by the opacity of crude oils and their emulsions and allows to determine the evolution of droplet size distribution (DSD) and the brine profile. This technique has been implemented to study the synergy of chemical demulsifiers and electric fields in the resolution of crude oil emulsion. Other techniques (electrorheology and critical electric field measurement) were also presented.

Finally, some industry-scale electrocoalescers were introduced and some examples of industrial implementation were presented.

Declaration of Competing Interest

The authors declare that they have no known competing financial interests or personal relationships that could have appeared to influence the work reported in this paper.

Acknowledgements

This review is, to a large extent, based on the experimental and theoretical work carried out in the Joint Industrial Consortium JIP Electrocoalescence Consortium, New Strategy for Separation of Complex Water-in-Crude Oil Emulsions: From Bench to Large Scale Separation (NFR Petromaks). Partners in this consortium were Ugelstad Laboratory

(NTNU, Norway), University of Alberta (Canada), Swiss Federal Institute of Technology in Zurich (ETH, Switzerland), Institutt for Energiteknikk (Norway). The activity was funded by Norwegian Research Council (NFR Grant No. 255174), and the following industrial companies: Anvendt Teknologi AS, Equinor, NalcoChampion, Nouryon, and Sulzer.

S. Simon thanks SUBPRO, a Research-based Innovation Centre within Subsea Production and Processing, for financing part of his position. SUBPRO is financed by the Research Council of Norway (Grant No. 237893), major industry partners (Aker Solutions, DNV-GL, Equinor, Kongsberg, Lundin Petroleum, Neptune Energy, TechnipFMC, and Total), and NTNU.

References

[1] Sjöblom J, Aske N, Harald Auflem I, Brandal O, Erik Havre T, Saether O, et al. Our current understanding of water-in-crude oil emulsions.: recent characterization techniques and high pressure performance. Adv Colloid Interface Sci 2003;100-102:399–473.
[2] Frising T, Noïk C, Dalmazzone C. The liquid/liquid sedimentation process: from droplet coalescence to technologically enhanced water/oil emulsion gravity separators: a review. J Dispers Sci Technol 2006;27(7):1035–57.
[3] Havre TE, Sjöblom J, Vindstad JE. Oil/water-partitioning and interfacial behavior of naphthenic acids. J Dispers Sci Technol 2003;24(6):789–801.
[4] Speight JG. Petroleum asphaltenes - Part 1: asphaltenes, resins and the structure of petroleum. Oil Gas Sci Technol 2004;59(5):467–77.
[5] Wang J, Buckley J. Effect of dilution ratio on amount of asphaltenes separated from stock tank oil. J Dispers Sci Technol 2007;28(3):425–30.
[6] Mullins OC. The modified yen model. Energy Fuel 2010;24(4):2179–207.
[7] Murgich J. Molecular simulation and the aggregation of the heavy fractions in crude oils. Mol Simul 2003;29(6–7):451–61.
[8] Chacón-Patiño ML, Rowland SM, Rodgers RP. Advances in asphaltene petroleomics. Part 3. Dominance of island or archipelago structural motif is sample dependent. Energy Fuel 2018;32(9):9106–20.
[9] Qiao P, Harbottle D, Tchoukov P, Masliyah J, Sjoblom J, Liu Q, et al. Fractionation of Asphaltenes in understanding their role in petroleum emulsion stability and fouling. Energy Fuel 2017;31(4):3330–7.
[10] Kilpatrick PK, Spiecker PM. Asphaltene emulsions. In: Sjöblom J, editor. Encyclopedic Handbook of emulsion technology. New York: Marcel Dekker, Inc.; 2001. p. 707–30.
[11] McLean JD, Kilpatrick PK. Effects of asphaltene aggregation in model heptane-toluene mixtures on stability of water-in-oil emulsions. J Colloid Interface Sci 1997;196(1):23–34.
[12] McLean JD, Kilpatrick PK. Effects of asphaltene solvency on stability of water-in-crude-oil Emulsions. J Colloid Interface Sci 1997;189(2):242–53.
[13] Pradilla D, Simon S, Sjöblom J. Mixed interfaces of asphaltenes and model demulsifiers part I: Adsorption and desorption of single components. Colloids Surf A Physicochem Eng Asp 2015;466(0):45–56.
[14] Structure function relations in asphaltenes and crude oils. In: Mullins O, Petroleomics C, Mullins OC, Hammami A, Marshall AG, editors. Asphaltenes, Heavy Oils, and Petroleomics. New York: Springer; 2007. p. 1–16.
[15] Rodgers RP, Schaub TM, Marshall AG. Petroleomics: MS returns to its roots. Anal Chem 2005;*77*(1) [20 A-27 A].
[16] Marshall AG, Rodgers RP. Petroleomics: the next grand challenge for chemical analysis. Acc Chem Res 2004;37(1):53–9.
[17] Xu Y, Dabros T, Hamza H, Shefantook W. Destabilization of water in bitumen emulsion by washing with water. Petrol Sci Technol 1999;17(9–10):1051–70.
[18] Spiecker PM, Gawrys KL, Trail CB, Kilpatrick PK. Effects of petroleum resins on asphaltene aggregation and water-in-oil emulsion formation. Colloids Surf A Physicochem Eng Asp 2003;220(1–3):9–27.
[19] Fan Y, Simon S, Sjoblom J. Influence of nonionic surfactants on the surface and interfacial film properties of asphaltenes investigated by Langmuir balance and Brewster angle microscopy. Langmuir 2010;26(13):10497–505.
[20] Lobato MD, Pedrosa JM, Hortal AR, Martínez-Haya B, Lebrón-Aguilar R, Lago S. Characterization and Langmuir film properties of asphaltenes extracted from Arabian light crude oil. Colloids Surf A Physicochem Eng Asp 2007;298(1–2):72–9.
[21] Lobato MD, Pedrosa JM, Mobius D, Lago S. Optical characterization of asphaltenes at the air/'water interface. Langmuir 2009;25(3):1377–84.
[22] Chang C-C, Nowbahar A, Mansard V, Williams I, Mecca J, Schmitt AK, et al. Interfacial rheology and heterogeneity of aging asphaltene layers at the water–oil interface. Langmuir 2018;34(19):5409–15.
[23] Nenningsland AL, Gao B, Simon S, Sjöblom J. Comparative study of stabilizing agents for water-in-oil emulsions. Energy Fuel 2011;25(12):5746–54.
[24] Jones TJ, Neustadter EL, Whittingham KP. Water-in-crude oil emulsion stability and emulsion destabilization by chemical demulsifiers. PETSOC-78-02-08 1978;*17*(02):10.
[25] Perles CE, Guersoni VCB, Bannwart AC. Rheological study of crude oil/water interface – the effect of temperature and brine on interfacial film. J Petrol Sci Eng 2018;162:835–43.
[26] Wang D, Lin M, Dong Z, Li L, Jin S, Pan D, et al. Mechanism of high stability of water-in-oil Emulsions at high temperature. Energy Fuel 2016;30(3):1947–57.
[27] Aryafar H, Kavehpour HP. Drop coalescence through planar surfaces. Phys Fluids 2006;18(7):072105.
[28] Aryafar H, Kavehpour HP. Electrocoalescence: effects of DC electric fields on coalescence of drops at planar interfaces. Langmuir 2009;25(21):12460–5.
[29] Taylor SE. Investigations into the electrical and coalescence behaviour of water-in-crude oil emulsions in high voltage gradients. Colloids Surf 1988;29(1):29–51.
[30] Mhatre S, Deshmukh S, Thaokar RM. Electrocoalescence of a drop pair. Phys Fluids 2015;27(9):092106.
[31] Karyappa Rahul B, Deshmukh Shivraj D, Thaokar Rochish M. Breakup of a conducting drop in a uniform electric field. J Fluid Mech 2014;754:550–89.
[32] Mhatre S, Vivacqua V, Ghadiri M, Abdullah AM, Al-Marri MJ, Hassanpour A, et al. Electrostatic phase separation: a review. Chem Eng Res Des 2015;96:177–95.
[33] Eastoe J, Dalton JS. Dynamic surface tension and adsorption mechanisms of surfactants at the air–water interface. Adv Colloid Interface Sci 2000;85(2–3):103–44.
[34] He Y, Yazhgur P, Salonen A, Langevin D. Adsorption–desorption kinetics of surfactants at liquid surfaces. Adv Colloid Interface Sci 2015;222:377–84.
[35] Lin S-Y, Lu T-L, Hwang W-B. Adsorption kinetics of decanol at the air-water Interface. Langmuir 1995;11(2):555–62.
[36] Ward AFH, Tordai L. Time dependence of boundary tensions of solutions I. the role of diffusion in time effects. J Chem Phys 1946;14(7):453–61.
[37] Hansen RS. The theory of diffusion controlled absorption kinetics with accompanying evaporation. J Phys Chem 1960;64(5):637–41.
[38] Van den Bogaert R, Joos P. Dynamic surface tensions of sodium myristate solutions. J Phys Chem 1979;83(17):2244–8.
[39] Rillaerts E, Joos P. Rate of demicellization from the dynamic surface tensions of micellar solutions. J Phys Chem 1982;86(17):3471–8.
[40] Serrien G, Joos P. Dynamic surface properties of aqueous sodium dioctyl sulfosuccinate solutions. J Colloid Interface Sci 1990;139(1):149–59.
[41] Joos P, Van Hunsel J. Adsorption kinetics of micellar Brij 58 solutions. Colloids Surf 1988;33:99–108.
[42] Lunkenheimer K, Serrien G, Joos P. The adsorption kinetics of octanol at the air/solution interface measured with the oscillating bubble and oscillating jet methods. J Colloid Interface Sci 1990;134(2):407–11.
[43] Fainerman VB, Makievski AV, Miller R. The analysis of dynamic surface tension of sodium alkyl sulphate solutions, based on asymptotic equations of adsorption kinetic theory. Colloids Surf A Physicochem Eng Asp 1994;87(1):61–75.
[44] Sjöblom J, Øye G, Glomm WR, Hannisdal A, Knag M, Brandal O, et al. Modern characterization techniques for crude oils, their emulsions, and functionalized surfaces. In: Sjöblom J, editor. Surfactant Science Series. Issue Emulsions and Emulsion Stability. 2nd ed., vol. 132. CRC Press LLC; 2006. p. 415–76.
[45] Chattoraj DK, Birdi K. S. Adsorption and the Gibbs Surface Excess. New York: Plenum Press; 1984. p. 471.
[46] Salager J-L. The fundamental basis for the action of a chemical dehydrant. Influence of the physical and chemical formulation on the stability of an emulsion. Int Chem Eng 1990;30:103–16.
[47] Angle CW. Chemical demulsification of stable crude oil and bitumen emulsions in petroleum recovery - a review. In: Sjöblom J, editor. Encyclopedic Handbook of Emulsion Technology. New York: Marcel Dekker; 2001. p. 541–94.
[48] Ese M-H, Galet L, Clausse D, Sjöblom J. Properties of Langmuir surface and interfacial films built up by asphaltenes and resins: influence of chemical demulsifiers. J Colloid Interface Sci 1999;220(2):293–301.
[49] Fan Y, Simon S, Sjoblom J. Interfacial shear rheology of asphaltenes at oil-water interface and its relation to emulsion stability: influence of concentration, solvent aromaticity and nonionic surfactant. Colloids Surf A 2010;366(1–3):120–8.
[50] Mohammed RA, Bailey AI, Luckham PF, Taylor SE. Dewatering of crude oil emulsions 1. Rheological behaviour of the crude oil—water interface. Colloids Surf A Physicochem Eng Asp 1993;80(2–3):223–35.
[51] Kim YH, Wasan DT. Effect of demulsifier partitioning on the destabilization of water-in-oil emulsions. Indust Eng Chem Res 1996;35(4):1141–9.
[52] Beetge JH. Emulsion stability studies based on the critical electric field (CEF) technique. Energy Fuel 2012;26(10):6282–91.
[53] Aske N, Kallevik H, Sjoblom J. Water-in-crude oil emulsion stability studied by critical electric field measurements. Correlation to physico-chemical parameters and near-infrared spectroscopy. J Petrol Sci Eng 2002;36(1–2):1–17.
[54] Mhatre S, Simon S, Sjöblom J, Xu Z. Demulsifier assisted film thinning and coalescence in crude oil emulsions under DC electric fields. Chem Eng Res Des 2018;134:117–29.
[55] Hjartnes TN, Mhatre S, Gao B, Sørland GH, Simon S, Sjöblom J. Demulsification of crude oil emulsions tracked by pulsed field gradient NMR. Part II: Influence of chemical demulsifiers in external AC electric field. Colloids Surf A Physicochem Eng Asp 2020;586:124188.
[56] Taylor GI, McEwan AD, de Jong LNJ. Studies in electrohydrodynamics. I. the circulation produced in a drop by an electric field. Proc R Soc Lond Ser A Math Phys Sci 1966;291(1425):159–66.
[57] Vizika O, Saville DA. The electrohydrodynamic deformation of drops suspended in liquids in steady and oscillatory electric fields. J Fluid Mech 1992;239:1–21.
[58] Torza S, Cox RG, Mason SG, Taylor GI. Electrohydrodynamic deformation and bursts of liquid drops. Philos Trans R Soc Lond Ser A Math Phys Sci 1971;269(1198):295–319.
[59] Lee SM, Im DJ, Kang IS. Circulating flows inside a drop under time-periodic nonuniform electric fields. Phys Fluids 2000;12(8):1899–910.
[60] Mhatre S, Simon S, Sjöblom J. Experimental evidence of enhanced adsorption dynamics at liquid–liquid interfaces under an electric field. Anal Chem 2020;92(19):12860–70.

[61] Ward T, Homsy GM. Electrohydrodynamically driven chaotic mixing in a translating drop. Phys Fluids 2001;13(12):3521–5.
[62] Ward T, Homsy GM. Electrohydrodynamically driven chaotic mixing in a translating drop. II Experiments. Phys Fluids 2003;15(10):2987–94.
[63] Morrison Jr FA. Transient heat and mass transfer to a drop in an electric field. J Heat Transfer 1977;99(2):269–73.
[64] Griffiths SK, Morrison Jr FA. Low peclet number heat and mass transfer from a drop in an electric field. J Heat Transfer 1979;101(3):484–8.
[65] Oliver DLR, Carleson TE, Chung JN. Transient heat transfer to a fluid sphere suspended in an electric field. Int J Heat Mass Transf 1985;28(5):1005–9.
[66] Oliver DLR, De Witt KJ. High Peclet number heat transfer from a droplet suspended in an electric field: interior problem. Int J Heat Mass Transf 1993;36 (12):3153–5.
[67] Christov CI, Homsy GM. Enhancement of transport from drops by steady and modulated electric fields. Phys Fluids 2009;21(8):083102.
[68] Hader MA, Jog MA. Effect of drop deformation on heat transfer to a drop suspended in an electrical field. J Heat Transfer 1998;120(3):682–9.
[69] Abdelaal MR, Jog MA. Steady and time-periodic electric field-driven enhancement of heat or mass transfer to a drop: internal problem. Int J Heat Mass Transf 2012;55(1):251–9.
[70] Abdelaal MR, Jog MA. Heat/mass transfer from a drop translating in steady and time-periodic electric fields: external problem. Int J Heat Mass Transf 2012;55(9): 2315–27.
[71] Abdelaal MR, Jog MA. Heat/mass transport in a drop translating in time-periodic electric fields. Int J Heat Mass Transf 2013;66:284–94.
[72] Chang LS, Carleson TE, Berg JC. Heat and mass transfer to a translating drop in an electric field. Int J Heat Mass Transf 1982;25(7):1023–30.
[73] Kaji N, Mori YH, Tochitani Y, Komotori K. Augmentation of direct-contact heat transfer to drops with an intermittent electric field. J Heat Transfer 1980;102(1): 32–7.
[74] He W, Baird MH, Chang JS. The effect of electric field on mass transfer from drops dispersed in a viscous liquid. Can J Chem Eng 1993;71(3):366–76.
[75] Weatherley LR, Petera J, Qiu Z. Intensification of mass transfer and reaction in electrically disturbed liquid-liquid systems. Chem Eng J 2017;322:115–22.
[76] Carleson TE. Drop oscillation and mass transfer in alternating electric fields. In: NASA STI/Recon Technical Report N. 1992; 1992. p. 17086.
[77] Schmid GM, Hurd RM, Snavely ES. Effects of electrostatic fields on the surface tension of salt solutions. J Electrochem Soc 1962;109(9):852.
[78] Hurd RM, Schmid GM, Snavely ES. Electrostatic fields: their effect on the surface tension of aqueous salt solutions. Science 1962;135(3506):791–2.
[79] Hayes CF. Water-air interface in the presence of an applied electric field. J Phys Chem 1975;79(16):1689–93.
[80] Moriya S, Adachi K, Kotaka T. Deformation of droplets suspended in viscous media in an electric field. 1. Rate of deformation. Langmuir 1986;2(2):155–60.
[81] Adachi K, Tanaka M, Shikata T, Kotaka T. Deformation of viscoelastic droplet in an electric field. 1. Aqueous cetyltrimethylammonium bromide-sodium salicylate solution in poly(dimethylsiloxane). Langmuir 1991;7(6):1281–6.
[82] Adachi K, Tanaka M, Kotaka T. Deformation of viscoelastic droplet in an electric field. 2. Aqueous poly(acrylamide) solution in poly(dimethylsiloxane). Langmuir 1991;7(6):1287–92.
[83] Moriya S, Kawamoto S, Urakawa O, Adachi K. Study of interfacial tension in poly (ethylene oxide)/polystyrene/diblock copolymer system by electric deformation method. Polymer 2006;47(17):6236–42.
[84] Degen P, Chen Z, Rehage H. Stimulated deformation of polysiloxane capsules in external electric fields. Macromol Chem Phys 2010;211(4):434–42.
[85] Morton SA, Keffer DJ, Counce RM, DePaoli DW. Behavior of oil droplets on an electrified solid metal surface immersed in ionic surfactant solutions. Langmuir 2005;21(5):1758–65.
[86] Santiago JM, Keffer DJ, Counce RM. Surfactant and electric field strength effects on surface tension at liquid/liquid/solid interfaces. Langmuir 2006;22(12): 5358–65.
[87] Mhatre S, Simon S, Sjöblom J. Shape evolution of a water drop in asphaltene solution under weak DC electric fields. Chem Eng Res Des 2019;141:540–9.
[88] Mhatre S, Simon S, Sjöblom J. Methodology to calculate interfacial tension under electric field using pendent drop profile analysis. Proc R Soc A Math Phys Eng Sci 2019;*475*(2225):20180852.
[89] Zeleny J. Instability of electrified liquid surfaces. Phys Ther Rev 1917;10(1):1–6.
[90] Mooney M. Variations in the cataphoretic mobilities of oil drops in water. Phys Ther Rev 1924;23(3):396–411.
[91] Nolan J. The breaking of water-drops by electric fields. Proc R Irish Acad Sec A Math Phys Sci 1926;37:28–39.
[92] Macky WA, Some Investigations. On the deformation and breaking of water drops in strong electric fields. Proc R Soc Lond Ser A Cont Pap Math Phys Char 1931; 133(822):565–87.
[93] Taylor G, Disintegration I. Of water drops in an electric field. Proc R Soc Lond Ser A Math Phys Sci 1964;280(1382):383–97.
[94] Allan RS, Mason SG, Marion LE. Particle behaviour in shear and electric fields I. deformation and burst of fluid drops. Proc R Soc Lond Ser A Math Phys Sci 1962; 267(1328):45–61.
[95] Dubash N, Mestel AJ. Breakup behavior of a conducting drop suspended in a viscous fluid subject to an electric field. Phys Fluids 2007;19(7):072101.
[96] Dubash N, Mestel AJ. Behaviour of a conducting drop in a highly viscous fluid subject to an electric field. J Fluid Mech 2007;581:469–93.
[97] Ha J-W, Yang S-M. Deformation and breakup of Newtonian and non-Newtonian conducting drops in an electric field. J Fluid Mech 2000;405:131–56.
[98] Karyappa RB, Thaokar RM. Electric-field-assisted formation of nonspherical microcapsules. Langmuir 2014;30(34):10270–9.
[99] Thaokar RM. Dielectrophoresis and deformation of a liquid drop in a non-uniform, axisymmetric AC electric field. Eur Phys J E 2012;35(8):76.
[100] Deshmukh SD, Thaokar RM. Deformation, breakup and motion of a perfect dielectric drop in a quadrupole electric field. Phys Fluids 2012;24(3):032105.
[101] Mhatre S, Thaokar R. Pin–plate electrode system for emulsification of a higher conductivity leaky dielectric liquid into a low conductivity medium. Indust Eng Chem Res 2014;53(34):13488–96.
[102] Karyappa RB, Naik AV, Thaokar RM. Electroemulsification in a uniform electric field. Langmuir 2016;32(1):46–54.
[103] Jung Y-M, Oh H-C, Kang IS. Electrical charging of a conducting water droplet in a dielectric fluid on the electrode surface. J Colloid Interface Sci 2008;322(2): 617–23.
[104] Im DJ, Noh J, Moon D, Kang IS. Electrophoresis of a charged droplet in a dielectric liquid for droplet actuation. Anal Chem 2011;83(13):5168–74.
[105] Mhatre S, Thaokar RM. Drop motion, deformation, and cyclic motion in a non-uniform electric field in the viscous limit. Phys Fluids 2013;25(7):072105.
[106] Pohl HA. Some effects of nonuniform fields on dielectrics. J Appl Phys 1958;29 (8):1182–8.
[107] Mhatre S, Thaokar R. Electrocoalescence in non-uniform electric fields: an experimental study. Chem Eng Process Process Intensification 2015;96:28–38.
[108] Mhatre S. Dielectrophoretic motion and deformation of a liquid drop in an axisymmetric non-uniform AC electric field. Sens Actuators B 2017;239: 1098–108.
[109] Im DJ, Kang IS. Electrohydrodynamics of a drop under nonaxisymmetric electric fields. J Colloid Interface Sci 2003;266(1):127–40.
[110] Dommersnes P, Rozynek Z, Mikkelsen A, Castberg R, Kjerstad K, Hersvik K, et al. Active structuring of colloidal armour on liquid drops. Nat Commun 2013;4(1): 2066.
[111] Sullivan AP, Kilpatrick PK. The effects of inorganic solid particles on water and crude oil emulsion stability. Ind Eng Chem Res 2002;41(14):3389–404.
[112] Ese M-H, Selsbak CM, Hannisdal A, Sjöblom J. Emulsions stabilized by indigenous reservoir particles: influence of chemical additive. J Dispers Sci Technol 2005;26 (2):145–54.
[113] Hannisdal A, Ese M-H, Hemmingsen PV, Sjoblom J. Particle-stabilized emulsions: effect of heavy crude oil components pre-adsorbed onto stabilizing solids. Colloids Surf A 2006;276(1–3):45–58.
[114] Langevin D, Poteau S, Henaut I, Argillier JF. Crude oil emulsion properties and their application to heavy oil transportation. Oil Gas Sci Technol 2004;59(5): 511–21.
[115] Nudurupati S, Janjua M, Singh P, Aubry N. Electrohydrodynamic removal of particles from drop surfaces. Phys Rev E 2009;80(1):010402.
[116] Nudurupati S, Janjua M, Singh P, Aubry N. Effect of parameters on redistribution and removal of particles from drop surfaces. Soft Matter 2010;6(6):1157–69.
[117] Chesters AK. The modelling of coalescence processes in fluid-liquid dispersions: a review of current understanding. Chem Eng Res Des 1991;69(4):259–70.
[118] Davis MH. Two charged spherical conductors in a uniform electric field: forces and field strength†. Q J Mech App Math 1964;17(4):499–511.
[119] Bird JC, Ristenpart WD, Belmonte A, Stone HA. Critical angle for electrically driven coalescence of two conical droplets. Phys Rev Lett 2009;103(16):164502.
[120] Roy S, Thaokar RM. Numerical study of coalescence and non-coalescence of two conducting drops in a non-conducting medium under electric field. J Electrostat 2020;108:103515.
[121] Anand V, Roy S, Naik VM, Juvekar VA, Thaokar RM. Electrocoalescence of a pair of conducting drops in an insulating oil. J Fluid Mech 2019;859:839–50.
[122] Luo X, Yin H, Ren J, Yan H, Lü Y, He L. Electrocoalescence criterion of conducting droplets suspended in a viscous fluid. J Phys Chem C 2019;123(32):19588–95.
[123] Anand V, Juvekar VA, Thaokar RM. An experimental study on the effect of conductivity, frequency and droplets separation on the coalescence of two aqueous drops under an electric field. Chem Eng Res Des 2019;152:216–25.
[124] Hasib R, Thaokar RM. An experimental study on the non-coalescence exhibited by anchored aqueous droplets in oil. Chem Eng Res Des 2020;161:103–14.
[125] Wang B-B, Wang X-D, Yan W-M, Wang T-H. Molecular dynamics simulations on coalescence and non-coalescence of conducting droplets. Langmuir 2015;31(27): 7457–62.
[126] Charles GE, Mason SG. The coalescence of liquid drops with flat liquid/liquid interfaces. J Colloid Sci 1960;15(3):236–67.
[127] Charles GE, Mason SG. The mechanism of partial coalescence of liquid drops at liquid/liquid interfaces. J Colloid Sci 1960;15(2):105–22.
[128] Blanchette F, Bigioni TP. Partial coalescence of drops at liquid interfaces. Nat Phys 2006;2(4):254–7.
[129] Thoroddsen ST, Takehara K. The coalescence cascade of a drop. Phys Fluids 2000; 12(6):1265–7.
[130] Mohamed-Kassim Z, Longmire EK. Drop coalescence through a liquid/liquid interface. Phys Fluids 2004;16(7):2170–81.
[131] Chen X, Mandre S, Feng JJ. Partial coalescence between a drop and a liquid-liquid interface. Phys Fluids 2006;18(5):051705.
[132] Chen X, Mandre S, Feng JJ. An experimental study of the coalescence between a drop and an interface in Newtonian and polymeric liquids. Phys Fluids 2006;18 (9):092103.
[133] Aryafar H, Kavehpour P. Electrocoalescence. Phys Fluids 2007;19(9):091107.
[134] Lukyanets AS, Kavehpour HP. Effect of electric fields on the rest time of coalescing drops. Appl Phys Lett 2008;93(19):194101.
[135] Hamlin BS, Creasey JC, Ristenpart WD. Electrically tunable partial coalescence of oppositely charged drops. Phys Rev Lett 2012;109(9):094501.

[136] Aryafar H, Kavehpour HP. Electrocoalescence fireworks. Phys Fluids 2010;22(9):091103.
[137] Hohman MM, Shin M, Rutledge G, Brenner MP. Electrospinning and electrically forced jets. I Stability theory. Phys Fluids 2001;13(8):2201–20.
[138] Atten P. Electrohydrodynamics of dispersed drops of conducting liquid: from drops deformation and interaction to Emulsion evolution. Int J Plasma Environ Sci Technol 2013;7(1):2–12.
[139] Hellesø SM, Atten P, Berg G, Lundgaard LE. Experimental study of electrocoalescence of water drops in crude oil using near-infrared camera. Exp Fluids 2015;56(6):122.
[140] Srivastava A, Karthick S, Jayaprakash KS, Sen AK. Droplet Demulsification using ultralow voltage-based Electrocoalescence. Langmuir 2018;34(4):1520–7.
[141] Mhatre S, Hjartnes T, Simon S, Sjöblom J. Coalescence behavior of stable pendent drop pairs held at different electric potentials. Langmuir 2020;36(7):1642–50.
[142] Weaver JC, Chizmadzhev YA. Theory of electroporation: a review. Bioelectrochem Bioenerg 1996;41(2):135–60.
[143] Thiam AR, Bremond N, Bibette J. Adhesive Emulsion bilayers under an electric field: from unzipping to fusion. Phys Rev Lett 2011;107(6):068301.
[144] Rekvig L, Kranenburg M, Vreede J, Hafskjold B, Smit B. Investigation of Surfactant efficiency using dissipative particle dynamics. Langmuir 2003;19(20):8195–205.
[145] Español P, Warren P. Statistical mechanics of dissipative particle dynamics. Europhys Lett 1995;30(4):191–6.
[146] Noid WG, Chu J-W, Ayton GS, Krishna V, Izvekov S, Voth GA, et al. The multiscale coarse-graining method. I. A rigorous bridge between atomistic and coarse-grained models. J Chem Phys 2008;*128*(24):244114.
[147] Skartlien R, Simon S, Sjöblom J. DPD molecular simulations of asphaltene adsorption on hydrophilic substrates: effects of polar groups and solubility. J Dispers Sci Technol 2016;37(6):866–83.
[148] Skartlien R, Simon S, Sjöblom J. Electrocoalescence of water in oil emulsions: a DPD simulation study and a novel application of electroporation theory. RSC Adv 2019;9(59):34172–83.
[149] Neu JC, Krassowska W. Asymptotic model of electroporation. Phys Rev E 1999;59(3):3471–82.
[150] Pradilla D, Simon S, Sjöblom J. Mixed interfaces of asphaltenes and model demulsifiers, part II: study of desorption mechanisms at liquid/liquid interfaces. Energy Fuel 2015;29(9):5507–18.
[151] Freeman SA, Wang MA, Weaver JC. Theory of electroporation of planar bilayer membranes: predictions of the aqueous area, change in capacitance, and pore-pore separation. Biophys J 1994;67(1):42–56.
[152] Anklam MR, Saville DA, Prud'homme RK. Stability and behavior of a comb–graft copolymer stabilizing a thin oil emulsion film. Polym Adv Technol 2001;12(1–2):70–84.
[153] Oleson TA, Sahai N, Wesolowski DJ, Dura JA, Majkrzak CF, Giuffre AJ. Neutron reflectivity study of substrate surface chemistry effects on supported phospholipid bilayer formation on (11$\bar{2}$0) sapphire. J Colloid Interface Sci 2012;370(1):192–200.
[154] Le Follotec A, Pezron I, Noik C, Dalmazzone C, Metlas-Komunjer L. Triblock copolymers as destabilizers of water-in-crude oil emulsions. Colloids Surf A Physicochem Eng Asp 2010;365(1):162–70.
[155] Croll AB, Dalnoki-Veress K. Hole nucleation in free-standing polymer membranes: the effects of varying molecular architecture. Soft Matter 2010;6(21):5547–53.
[156] Chang C-L, Fogler HS. Stabilization of asphaltenes in aliphatic solvents using alkylbenzene-derived amphiphiles. 2. Study of the asphaltene-amphiphile interactions and structures using Fourier transform infrared spectroscopy and small-angle X-ray scattering techniques. Langmuir 1994;10(6):1758–66.
[157] Amirfazli A, Neumann AW. Status of the three-phase line tension: a review. Adv Colloid Interface Sci 2004;110(3):121–41.
[158] Alarcón F, Pérez E, Gama Goicochea A. Dissipative particle dynamics simulations of weak polyelectrolyte adsorption on charged and neutral surfaces as a function of the degree of ionization. Soft Matter 2013;9(14):3777–88.
[159] Lee M-T, Vishnyakov A, Neimark AV. Modeling proton dissociation and transfer using dissipative particle dynamics simulation. J Chem Theory Comput 2015;11(9):4395–403.
[160] Skartlien R, Bertheussen A, Simon S, Sjöblom J. Development of electrochemical DPD molecular simulations for oil/water partitioning of organic acids at varying pH. J Dispers Sci Technol 2018;39(9):1367–75.
[161] Groot RD. Electrostatic interactions in dissipative particle dynamics—simulation of polyelectrolytes and anionic surfactants. J Chem Phys 2003;118(24):11265–77.
[162] Li X, Liu Y, Tang J, Li S. Dissipative particle dynamics simulation of wettability alternation phenomena in the chemical flooding process. Acta Mechanica Sinica 2009;25(5):583–7.
[163] Keleşoğlu S, Barrabino A, Sørland G, Simon S, Paso K, Sjöblom J. Rheological properties of dense packed layer (DPL) of Asphaltene stabilized Emulsions. J Petrol Sci Eng 2015;126:1–10.
[164] Czarnecki J, Moran K, Yang X. On the "rag layer" and diluted bitumen froth dewatering. Can J Chem Eng 2007;85(5):748–55.
[165] Grimes BA, Dorao CA, Opedal NVDT, Kralova I, Sørland GH, Sjöblom J. Population balance model for batch gravity separation of crude oil and water Emulsions. Part II: comparison to experimental crude oil separation data. J Dispers Sci Technol 2012;33(4):591–8.
[166] Opedal N, Kralova I, Lesaint C, Sjöblom J. Enhanced sedimentation and coalescence by chemicals on real crude oil systems. Energy Fuel 2011;25(12):5718–28.
[167] Opedal N, Sørland G, Sjöblom J. Emulsion Stability studied by nuclear magnetic resonance (NMR). Energy Fuel 2010;24(6):3628–33.
[168] Jerschow A, Müller N. Convection compensation in gradient enhanced nuclear magnetic resonance spectroscopy. J Magn Reson 1998;132(1):13–8.
[169] Sørland GH. Dynamic Pulsed-Field-Gradient NMRvol. 110. Berlin Heidelberg: Springer-Verlag; 2014. p. 354.
[170] Mitra PP, Sen PN, Schwartz LM. Short-time behavior of the diffusion coefficient as a geometrical probe of porous media. Phys Rev B 1993;47(14):8565.
[171] Hurlimann MD, Helmer KG, Latour LL, Sotak CH. Restricted diffusion in sedimentary rocks. Determination of surface-area-to-volume ratio and surface relaxivity. J Magn Reson A 1994;111(2):169–78.
[172] Uh J, Watson AT. Nuclear magnetic resonance determination of surface relaxivity in permeable media. Indust Eng Chem Res 2004;43(12):3026–32.
[173] Meiboom S, Gill D. Modified spin-echo method for measuring nuclear relaxation times. Rev Sci Instrum 1958;29(8):688–91.
[174] Cohen MH, Mendelson KS. Nuclear magnetic relaxation and the internal geometry of sedimentary rocks. J Appl Phys 1982;53(2):1127–35.
[175] Carr HY, Purcell EM. Effects of Diffusion on Free Precession in Nuclear Magnetic Resonance Experiments. Physical Review 1954;94(3):630–8.
[176] Hjartnes TN, Sørland GH, Simon S, Sjöblom J. Demulsification of crude oil emulsions tracked by pulsed field gradient (PFG) nuclear magnetic resonance (NMR). Part I: chemical demulsification. Indust Eng Chem Res 2019;58(6):2310–23.
[177] Hannisdal A, Hemmingsen PV, Silset A, Sjöblom J. Stability of water/crude oil systems correlated to the physicochemical properties of the oil phase. J Dispers Sci Technol 2007;28(4):639–52.
[178] Coutinho RCC, Pinto JC, Nele M, Hannisdal A, Sjöblom J. Evaluation of water-in-crude-oil emulsion stability using critical electric field: effect of emulsion preparation procedure and crude oil properties. J Dispers Sci Technol 2011;32(7):923–34.
[179] Hemmingsen PV, Silset A, Hannisdal A, Sjoblom J. Emulsions of heavy crude oils I: influence of viscosity, temperature and dilution. J Dispers Sci Technol 2005;26:615–27.
[180] Yang X, Verruto VJ, Kilpatrick PK. Dynamic asphaltene-resin exchange at the oil/water Interface: time-dependent W/O emulsion stability for asphaltene/resin model oils. Energy Fuel 2007;21(3):1343–9.
[181] Lesaint C, Glomm WR, Lundgaard LE, Sjöblom J. Dehydration efficiency of AC electrical fields on water-in-model-oil emulsions. Colloids Surf A Physicochem Eng Asp 2009;352(1–3):63–9.
[182] Less S, Hannisdal A, Sjöblom J. An electrorheological study on the behavior of water-in-crude oil emulsions under influence of a DC electric field and different flow conditions. J Dispers Sci Technol 2008;29(1):106–14.
[183] Noik C, Chen J, Dalmazzone CSH. Electrostatic demulsification on crude oil: a state-of-the-art review. In: International Oil & Gas Conference and Exhibition in China, SPE-103808-MS. Beijing, China: Society of Petroleum Engineers; 2006. p. 12.
[184] Urdahl O, Nordstad K, Berry P, Wayth N, Williams T, Bailey A, et al. Development of a new, compact electrostatic coalescer concept. SPE-69196-PA 2001;*16*(01):4–8.
[185] Amarzguioui M, Jacobsen PC. Overcoming separation challenges by use of electrocoalescence technology. In: SPE Asia Pacific Oil & Gas Conference and Exhibition, SPE-171483-MS. Adelaide, Australia: Society of Petroleum Engineers; 2014. p. 14.
[186] Al-Qahtani AA. Vessel Internal Electrostatic Coalescer technology (VIEC). In: SPE International Production and Operations Conference & Exhibition, SPE-156087-MS. Doha, Qatar: Society of Petroleum Engineers; 2012. p. 9.
[187] Less S, Hannisdal A, Bjørklund E, Sjöblom J. Electrostatic destabilization of water-in-crude oil emulsions: application to a real case and evaluation of the Aibel VIEC technology. Fuel 2008;87(12):2572–81.
[188] Chiesa M, Abd Elhamid WT. New separation technology. In: Abu Dhabi International Petroleum Exhibition and Conference, SPE-136836-MS. Abu Dhabi, UAE: Society of Petroleum Engineers; 2010. p. 7.
[189] Grave EJ, Olson MD, Menchaca AE, Westra RW, Akdim MR. Performance testing of an inline electrocoalescer device with medium and heavy crudes. SPE-174090-PA 2015;*4*(05):56–65.
[190] Fjeldly TA, Hansen EB, Nilsen PJ. Novel coalescer technology in first-stage separator enables one-stage separation and heavy-oil separation. In: Offshore Technology Conference, OTC-18278-MS; Offshore Technology Conference: Houston, Texas, USA; 2006. p. 6.
[191] Wolff EA, Knutsen TL, Piasecki WA, Hansson P, Nilsen PJ. Advanced Electrostatic Internals in the 1st Stage Separator Enhance Oil/Water Separation and Reduce Chemical Consumption on the Troll C Platform. In: Offshore Technology Conference, OTC-16321-MS; Offshore Technology Conference: Houston, Texas; 2004. p. 7.
[192] Sulzer. https://www.sulzer.com/-/media/files/products/separation-technology/separators/viec_vessel_internal_electrostatic_coalescer.ashx?la=en [accessed 25/10/2020].